Accepted Manuscript

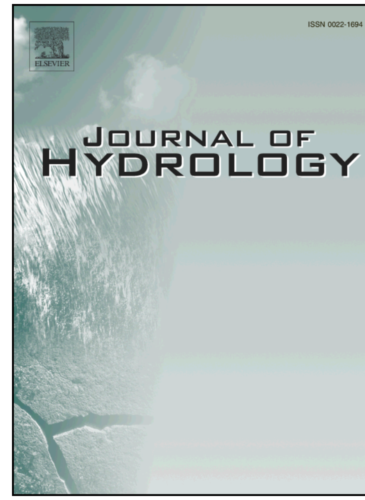

Research papers

A Two-update Ensemble Kalman Filter for Land Hydrological Data Assimilation with an Uncertain Constraint

M. Khaki, B. Ait-El-Fquih, I. Hoteit, E. Forootan, J. Awange, M. Kuhn

PII: S0022-1694(17)30707-2
DOI: https://doi.org/10.1016/j.jhydrol.2017.10.032
Reference: HYDROL 22312

To appear in: *Journal of Hydrology*

Received Date: 7 June 2017
Revised Date: 16 October 2017
Accepted Date: 17 October 2017

A Two-update Ensemble Kalman Filter for Land Hydrological Data Assimilation with an Uncertain Constraint

M. Khaki[a,1], B. Ait-El-Fquih[b], I. Hoteit[b], E. Forootan[c], J. Awange[a], M. Kuhn[a]

[a] *Department of Spatial Sciences, Curtin University, Perth, Australia.*

[b] *King Abdullah University of Science and Technology (KAUST), Thuwal, Saudi Arabia.*

[c] *School of Earth and Ocean Sciences, Cardiff University, Cardiff, UK.*

Abstract

Assimilating Gravity Recovery And Climate Experiment (GRACE) data into land hydrological models provides a valuable opportunity to improve the models' forecasts and increases our knowledge of terrestrial water storages (TWS). The assimilation, however, may harm the consistency between hydrological water fluxes, namely precipitation, evaporation, discharge, and water storage changes. To address this issue, we propose a weak constrained ensemble Kalman filter (WCEnKF) that maintains estimated water budgets in balance with other water fluxes. Therefore, in this study, GRACE terrestrial water storages data are assimilated into the World-Wide Water Resources Assessment (W3RA) hydrological model over the Earth's land areas covering 2002 – 2012. Multi-mission remotely sensed precipitation measurements from the Tropical Rainfall Measuring Mission (TRMM) and evaporation products from the Moderate Resolution Imaging Spectroradiometer (MODIS), as well as ground-based water discharge measurements are applied to close the water balance equation. The proposed WCEnKF contains two update steps; first, it incorporates observations from GRACE to improve model simulations of water storages, and second, uses the additional observations of precipitation, evaporation, and water discharge to establish the water budget closure. These steps are designed to account for error information associated with the included observation sets during the assimilation process. In order to evaluate the assimilation results, in addition to monitoring the water budget closure errors, in-situ groundwater measurements over the Mississippi River Basin in the US and the Murray-Darling Basin in Australia are used. Our results indicate approximately 24% improvement in the WCEnKF groundwater estimates over both basins compared to the use of (constraint-free) EnKF. WCEnKF also further reduces imbalance errors by approximately 82.53% (on average) and at the same time increases the correlations between the assimilation solutions and the water fluxes.

Email address: Mehdi.Khaki@postgrad.curtin.edu.au (M. Khaki)

[1] Contact details: Department of Spatial Sciences, Curtin University, Perth, Australia, Email: Mehdi.Khaki@postgrad.curtin.edu.au, Tel: 0061410620379

Keywords: Constrained data assimilation, Ensemble Kalman filtering, Weak constrained ensemble Kalman filter, Water budget closure, Hydrological modelling.

1. Introduction

Terrestrial water storage plays an important role in both human life and environment all around the world. Quantifying this major water resource is, therefore, essential and can be done using different tools including ground-based in-situ measurements, satellite remote sensing data, and hydrological models. In the last few decades, hydrological models have extensively been used to determine and monitor stored water and fluxes in different forms within landscapes such as ice and snow, glaciers, aquifers, soils, and surface waters (e.g., Chiew et al., 1993; Wooldridge and Kalma, 2001; Döll et al., 2003; Huntington, 2006; van Dijk, 2010). The models have been designed to reflect the behavior of a system of interest while satisfying known physical properties reliably (Smith et al., 2011). However, various sources of uncertainty, due for example, imperfect modeling, data limitations on both temporal and spatial resolutions, errors in forcing fields, as well as empirical model parameters, limit the accuracy of hydrological models (Vrugt et al., 2013; van Dijk et al., 2011, 2014). Assimilating accurate observations into models is an effective approach to overcome these limitations (e.g., McLaughlin, 2002; Zaitchik et al., 2008; van Dijk et al., 2014; Gharamti et al., 2016).

Data assimilation is a procedure for incorporating observations of one or more variables (according to their uncertainties) into a numerical (physical) model to increase consistency of model simulations of a certain variable with its changes in the 'real world' (Bertino et al., 2003; Hoteit et al., 2012). Therefore it has been widely applied in hydrological studies to improve different water compartments, such as soil moisture (e.g., Reichle et al., 2002; Brocca et al., 2010; Renzullo et al., 2014), surface water (e.g., Alsdorf et al., 2007; Neal et al., 2009; Giustarini et al., 2011), and snow storages (e.g., Liu et al., 2013; Kumar et al., 2015). During past few years, some studies have assessed the capability of Gravity Recovery And Climate Experiment (GRACE) data, available since March 2002, to improve terrestrial water storages (TWS) (e.g., Zaitchik et al., 2008; Eicker et al., 2014; Tangdamrongsub et al., 2015; Schumacher et al., 2016; Tangdamrongsub et al., 2017; Khaki et al., 2017a,b; Tian et al., 2017) simulated by land (surface) hydrological models.

The water balance equation is applied in land hydrological models to describe the relationships between changes in water storage ($\Delta\mathbf{s}$), evaporation ($\mathbf{e}$), precipitation ($\mathbf{p}$), and discharge ($\mathbf{q}$), i.e., $\Delta\mathbf{s} = \mathbf{p} - \mathbf{e} - \mathbf{q}$ (Sokolov and Chapman, 1974). However, the application of data assimilation may destroy the dynamical balances between water fluxes and water storage changes (Pan and Wood, 2006). In another words, models water storage states are in balance since model structure, e.g., its equations, governs variations in the water state changes due to the incoming and outgoing hydrological water fluxes. An assimilation of water storage states (e.g., GRACE data) does not constraint the assimilated state to be balanced. Eicker et al. (2016) found distinct changes in the linear rates and seasonality of water storage from GRACE and the flux deficit ($\mathbf{p} - \mathbf{e} - \mathbf{q}$) even over large-scale river basins. Therefore, after assimilation, one can expect mismatches between the model estimation of $\Delta\mathbf{s}$ and the flux deficit after each assimilation cycle. This issue must be mitigated to better interpret model derived water storage changes after implementing data assimilation (see, e.g., Roads et al., 2003; Pan and Wood, 2006; Sahoo et al., 2011).

In order to enhance the estimation of model water storages (e.g., for $\Delta\mathbf{s}$), it is important that the water variables satisfy the water closure equation. One way to do this is to impose a balance constraint based on the water budget equation after each assimilation cycle (Pan et al., 2012). Few assimilation schemes have been proposed in this context. Pan and Wood (2006) developed a constrained ensemble Kalman filter (CEnKF) based on the ensemble Kalman filter (EnKF; Evensen, 1994) to solve the disclosure of the water balance equation after implementing a data assimilation over the southern Great Plains region of the United States. In addition to using CEnKF, Sahoo et al. (2011) and Pan et al. (2012) applied a data merging algorithm to prepare the datasets for data assimilation and to check for imbalance over various major river basins. They merged data from different sources (e.g., in situ observations, remote sensing retrievals, land surface model simulations, and global reanalyses) so that their errors can be used to achieve optimal weights leading to the best estimates for each terrestrial water cycle. These data were then used to resolve water balance errors by applying CEnKF (see also Zhang et al., 2016). In these studies, information about the uncertainties associated with water balance observations, however, have not been incorporated during data assimilation. The strong constraint imposed by assuming observation to be perfect is unrealistic and can cause estimation errors such as over-fitting issues (Tangdamrongsub et al., 2017). This motivates the new filtering technique, which is proposed in this study to involve observation errors in the assimilation procedure.

In this study, a new constrained ensemble Kalman filter, which we refer to as weak constrained ensemble Kalman filter (WCEnKF), is introduced that satisfies the closure of the water balance equation while taking the uncertainties in datasets into the account. WCEnKF is formulated based on the EnKF and imposes the closure constraint as a second update step, where the EnKF analysis members are updated to remain in balance with other variables (hereafter called pseudo-observation, and includes **p**, **e**, and **q** through the water balance equation). Water storages are therefore first updated using GRACE observations as in the EnKF in the first step, and the broken water balance is then mitigated using the pseudo-observations in the second EnKF update step. The novelty of the proposed scheme is that it accounts for the uncertainties in the pseudo-observations so that the budget closure is not strongly imposed. Moreover, in contrast to existing schemes, the filter does not seek to redistribute the imbalance between all compartments (i.e., Δs, **p**, **e**, and **q**) and only adjusts the already estimated water storage ($\Delta\mathbf{s}$). WCEnKF treats **p**, **e**, and **q** and their uncertainties as a new set of observations, similar to any other observation in a standard EnKF. The imbalance problem requires a particular formulation of the state-space system, for which the process does not only depend on the state at the filtering time but also on the previous time.

The proposed WCEnKF with the dual update steps is used to assimilate GRACE TWS data into the World-Wide Water Resources Assessment (W3RA) hydrological model globally during 2002 – 2012. In addition to GRACE TWS data, remotely sensed measurements of **p** and **e** are also used to constrain the water balance in the filter estimates. For this purpose, we use the Tropical Rainfall Measuring Mission (TRMM-3B43; Huffman et al., 2007) precipitation products for **p**, the Moderate Resolution Imaging Spectroradiometer (MODIS) evaporation data (MOD16; Mu et al., 2007) for **e**, and the water discharge measurements from various ground stations for **q**. Although the imbalance constraint is spatially limited to locations, where ground-based discharge data are available, the Kalman-like second update step of WCEnKF spreads the imbalance adjustments to all model grid points. For a better presentation of results, we choose eight globally distributed major basins with a dense network of water discharge measurements and analyze the assimilation solution separately over each basin. Among these basins, the Mississippi River Basin and the Murray-Darling Basin are selected subject to the availability of ground-based data to evaluate the performance of WCEnKF against in-situ groundwater measurements.

The remainder of this paper is organized as follows. We first describe the model and data in Section 2. The filtering technique and the data assimilation setup are then described in Section 3. Section 4 presents the assimilation results, analyses the filter estimates and water budget closure (Subsection 4.3), and evaluates the estimates against in-situ data (Subsection 4.2). Finally, summary and conclusions are provided in Section 5.

2. Model and Data

2.1. W3RA Hydrological Model

We use a grid distributed biophysical model of W3RA from the Commonwealth Scientific and Industrial Research Organisation (CSIRO). The model is designed to simulate landscape water stored in the vegetation and soil systems (van Dijk, 2010). The $1^{\circ}\times1^{\circ}$ version of W3RA is applied to represent the water balance of the soil, groundwater and surface water stores, in which each cell is modeled independently from its neighbors (van Dijk, 2010; Renzullo et al., 2014). The model parameters include effective soil parameters, water holding capacity and soil evaporation, relating greenness and groundwater recession, and saturated area to catchment characteristics (van Dijk et al., 2013). Forcing datasets consist of the daily meteorological fields of minimum and maximum temperature, downwelling short-wave radiation, and precipitation by Princeton University (Sheffield et al., 2006). The model state is composed of storages of the top, shallow root and deep root soil layers, groundwater storage, and surface water storage. The simulation covers the period from April 2002 to December 2012.

W3RA represents the storage of water in small river channels and consequently surface water storage changes in reservoir and lakes are not simulated by the model. Therefore, it is necessary to remove surface water storages from GRACE TWS data before assimilation even though it has much lesser effects than other water storages such as groundwater and soil moisture. For this purpose, we use the WaterGAP Global Hydrology Model (WGHM; more details on Döll et al., 2003) surface storage estimations. WGHM models the vertical and horizontal water fluxes on a $0.5^{\circ}\times0.5^{\circ}$ grid resolution and describes the major hydrological components, such as snow accumulation, runoff, and the lateral transport of water within the river networks (Forootan et al., 2014). The surface water storages from WGHM are removed from the GRACE TWS before assimilation. Note that after updating the model states using the adjusted GRACE data (first update step in WCEnKF), the removed surface water storages are added to the filtered TWS estimates before applying the water budget closure step (second update step).

2.2. Terrestrial Water Storage (TWS) Data

Monthly TWS derived from GRACE level 2 (L2) gravity field data are used in the first step of the proposed filtering scheme to update the summation of the model derived water storage simulations including top soil, shallow soil, deep soil water, snow, vegetation, and groundwater. GRACE data are provided in terms of the gravity potential Stokes' coefficients, truncated at spherical harmonic degree and order 90, together with their full error information from the ITSG-Grace2016 gravity field model (Mayer-Gürr et al., 2014). Some post-processing steps are applied on the coefficients before converting them into TWSs. Degree 1 and degree 2 (C20) coefficients are replaced by more accurate coefficients that are calculated by Swenson et al. (2008) and the Satellite Laser Ranging solutions (Cheng and Tapley, 2004), respectively. We also apply DDK2 (Kusche et al., 2009) to mitigate colored/correlated noise in the coefficients. The L2 gravity fields are then converted to $1°\times1°$ TWS fields following Wahr et al. (1998). The mean TWS is taken from the model for the study period and is added to the GRACE TWS change time series to obtain absolute values in accordance with W3RA (Zaitchik et al., 2008). We further exploit the provided full error information of the Stokes' coefficients to construct an observation error covariance matrix for data assimilation. This is done by converting GRACE spherical harmonic error coefficients to error covariances associated with TWS data as suggested by Eicker et al. (2014) and Schumacher et al. (2016). Eicker et al. (2014) showed that applying GRACE TWS data on a $1°\times1°$ grid resolution results in a rank deficiency problem during data assimilation (see also Khaki et al., 2017b). However, as shown by Khaki et al. (2017b), the application of local analysis (LA) successfully mitigates this problem by spatially limiting the use of ensemble-based covariance information in high-dimensional systems. Therefore, here, we follow Khaki et al. (2017b) and apply LA to cope with rank deficiency problem (see details in Section 3.3).

2.3. Water Fluxes

Precipitation data of TRMM-3B43 products (TRMM, 2011; Huffman et al., 2007) is used. This dataset is limited spatially between 50°N and 50°S in latitude, and $-180°$ to $+180°$ in longitude. The data is re-sampled from $0.25°\times0.25°$ to a monthly $1°\times1°$ spatial resolution. We also use the relative error available for each gridpoint and different times (Huffman et al., 1997).

We also acquire MOD16 evaporation data from the University of Montana's Numerical Terradynamic Simulation group with eight days temporal resolution and one km spatial resolution

(Mu et al., 2011). The gridded data is converted to a monthly temporal scale and $1^{\circ}\times1^{\circ}$ spatial resolution. Following Aires (2014) and Munier et al. (2014), 10 mm uncertainty is considered for the evaporation data.

Different data sources are used to provide water discharge data with a maximum global coverage. In this regard, the largest part of runoff products (1970 globally distributed stations) is acquired from the Global Runoff Data Centre (GRDC). Over Africa, 83 stations are obtained from SIEREM (Systeme d'Informations Environnementales sur les Ressources en Eau et leur Modelisation), an environmental information system for water resources (Boyer et al., 2006). In additions, two dense networks of discharge stations over the United State (3800 stations), Southeast Asia (1700 stations), and Australia (1250 stations) are provided from the United States Geological Survey (USGS), China Hydrology Data Project (Henck et al., 2010; Schmidt et al., 2011), and the Australian Bureau of Meteorology under the Water Regulations (2008). In addition, a number of discharge stations are also obtained from the National River Flow Archive (NRFA), Department of Hydrology and Meteorology of Nepal, the Hydrology and Geochemistry of the Amazon basin (HYBAM) for the Amazon, Orinoco, and Congo basins. Figure 1 shows the locations of discharge stations distributed globally.

As mentioned, the water budget closure relies on $\mathbf{p}$, $\mathbf{e}$, and $\mathbf{q}$. Wherever a discharge station is located, it is possible to impose water budget closure adjustment. At each $1^{\circ}\times1^{\circ}$ grid point we use the nearest discharge stations to spatially interpolate the observations $\mathbf{q}$. To this end, an average of data from discharge stations located within 0.5° radius of each grid point is assigned to this grid point. Since no straight information on the data uncertainty is available, two approaches are applied here to specify errors on the data. Sheffield et al. (2009) suggested that the standard errors in the gauge-based data are 5% to 10% of the discharge values and Pan et al. (2012) proposed a formula to estimate the discharge error for a basin within a given area A as,

$$Relative\,Error\,(\%) = 5\frac{(A_1 - A)}{(A_1 - A_2)} + 5, \tag{1}$$

where A_1 and A_2 are the areas of Amazon Basin ($4.62 \times 10^6 km^2$) and Ural Basin ($0.19 \times 10^6 km^2$), respectively. Here we use eq. (1) to assign errors to discharge stations located in the major basins of Amazon, Indus, Mississippi, Orange, Danube, St. Lawrence, Murray-Darling, and Yangtze, and 10% of discharge value for any station outside of these areas as suggested by literature (e.g., Pan et al., 2012; Aires, 2014; Munier et al., 2014).

FIGURE 1

2.4. In-situ Measurements

In addition to monitoring water budget closure errors using the water fluxes observations, we use in-situ groundwater measurements over the Mississippi Basin and Murray-Darling Basin to evaluate the performance of the proposed filter. The distribution of groundwater well stations is presented in Figure 2. In the Mississippi Basin, independent data are collected from USGS. Additional measurements are provided for the Murray-Darling Basin by the New South Wales Government (NSW) groundwater archive. Monthly well measurements are acquired and time series of groundwater storage anomalies are generated. Generally, a specific yield is required to convert well-water levels to variations in groundwater storage regarding equivalent water heights (Rodell et al., 2007; Zaitchik et al., 2008). This information, however, is not available in our case, so TWS variation from GRACE and Global Land Data Assimilation System (GLDAS) soil moisture are used to calculate the specific yield and scale the observed headwater by modifying the magnitude of groundwater time series (Tregoning et al., 2012; Tangdamrongsub et al., 2015). As Tregoning et al. (2012) showed, the GW component can be extracted by removing the soil moisture component from GRACE TWS data while other compartments like biomass and surface water variations can be excluded due to their small contribution to regional scale mass variations. The calculated specific yields range between 0.08 and 0.16 over the Murray-Darling Basin, falling within the 0.05–0.2 range suggested by the Australian Bureau of Meteorology (BOM) and Seoane et al. (2013), and range between 0.15 and 0.22 over the Mississippi Basin along with those suggested by Gutentag et al. (1984) (i.e., 0.1 to 0.3), thereby justifying the application of the method. Using extracted yield factors, one can extract the groundwater components from the measured well-water levels. The scaled groundwater time series are then used to evaluate the data assimilation results over each basin. To this end, we compare groundwater estimates after data assimilation with ground-based groundwater measurements. Details of the datasets used in this study are outlined in Table 1.

FIGURE 2

TABLE 1

3. The Weak Constrained Ensemble Kalman Filter (WCEnKF)

3.1. Problem Formulation

Let $\{\mathbf{x}_t\}_{t=0}^{T} \in \mathbb{R}^{n_x}$ denote the (unknown) system state process formed by top soil, shallow soil, deep soil water, snow, vegetation, and groundwater. Note that except for groundwater, all the other components are simulated with two hydrological response units (HRU) of tall, e.g., deep-rooted vegetation and short, e.g., shallow-rooted vegetation, which leads to 11 state variables $(5 \times 2 + 1)$ of W3RA at each grid cell (24509 cells in total). Although in general, t refers to model time steps, for the sake of simplicity, we assume that the model time step is equal to the assimilation time step (monthly scale). $\{\mathbf{y}_t\}_{t=0}^{T} \in \mathbb{R}^{n_y}$ represents the GRACE TWS observed process. The state and observed processes are related through a dynamical state-space system of the form,

$$\begin{cases} \mathbf{x}_t &= \mathcal{M}_{t-1}(\mathbf{x}_{t-1}) + \nu_t, \\ \mathbf{y}_t &= \mathbf{H}_t \mathbf{x}_t + \mathbf{w}_t, \end{cases} \tag{2}$$

for which the state transition operator, $\mathcal{M}(.)$, is nonlinear. $\mathbf{H}$ is the (observation) design matrix containing 11 ones in each of the 24509 rows, representing the sum of the individual compartments to TWS at each grid cell with all the other elements of the rows being zero (total 269599 columns). The proposed scheme can be easily extended to the case of nonlinear observation operator (i.e., in which $\mathbf{H}_t\mathbf{x}_t$ is replaced by $h_t(\mathbf{x_t})$), as for example discussed in Liu and Xue (2002). The state transition noise process, $\nu = \{\nu_t\}_t$, and the observation noise process, $\mathbf{w} = \{\mathbf{w}_t\}_t$, are assumed to be independent, jointly independent, and independent of the initial state, $\mathbf{x}_0$. Furthermore, $\mathbf{x}_0$, ν_t, and $\mathbf{w}_t$ are assumed to be Gaussian; ν_t and $\mathbf{w}_t$ with zero mean and covariances $\mathbf{Q}_t$ and $\mathbf{R}_t$, respectively.

Data assimilation can destroy the balance between water fluxes. It is therefore essential to incorporate the water balance equation by imposing an equality constraint to restore the balance problem. Changes in monthly mean water storage at two different time steps (e.g., t and $t-1$) should be equal, up to uncertainties in the involved data, to the difference between the monthly mean input ($\mathbf{p}$) and output ($\mathbf{e}$ and $\mathbf{q}$) water storages. This can be formulated as:

$$\mathbf{d}_t = -\mathbf{x}_t + \mathbf{x}_{t-1} + \mathbf{p}_t - \mathbf{e}_t - \mathbf{q}_t + \boldsymbol{\xi}_t, \tag{3}$$

where $\{\boldsymbol{\xi}_t\}_t$ is the noise process accounting for errors associated with the different water fluxes data. Here we assume $\boldsymbol{\xi}_t$ Gaussian white noise with zero mean and covariance $\boldsymbol{\Sigma}_t$, and independent of $\mathbf{x}_0$ and $\{\mathbf{w}_t\}_t$. Defining $\mathbf{z}_t = \mathbf{d}_t - \mathbf{p}_t + \mathbf{e}_t + \mathbf{q}_t$, the constraint eq. (3) is rewritten as,

$$\mathbf{z}_t = \mathbf{G}\mathbf{x}_t + \mathbf{L}\mathbf{x}_{t-1} + \boldsymbol{\xi}_t, \tag{4}$$

where $\mathbf{G}$, in general, is the $n_x \times n_x$ (with n_x being the length of x) identity matrix while in this study $\mathbf{G} = \mathbf{H}$ to aggregate different water compartments at each grid point and $\mathbf{L} = -\mathbf{G}$.

In the constrained state-space system eqs. (2) – (4), we focus on the filtering problem, say, on the estimation, at each time t, of the system state, $\mathbf{x}_t$, conditional on both GRACE TWS observations, $\mathbf{y}_{0:t} \stackrel{\text{def}}{=} \{\mathbf{y}_0, \mathbf{y}_1, \cdots, \mathbf{y}_t\}$ and "pseudo-observations" $\mathbf{z}_{0:t}$. Let $\mathbf{r}_t = [\mathbf{y}_t^T, \mathbf{z}_t^T]^T$. As known in the Bayesian estimation theory, the computation of any estimator of $\mathbf{x}_t$ from $\mathbf{r}_{0:t}$ is based on the so-called posterior (filtering or analysis) probability density function (pdf), $p(\mathbf{x}_t|\mathbf{r}_{0:t})$. For instance, the posterior mean (PM) estimator, $\hat{\mathbf{x}}_{t|t}$, which minimizes the mean squared error, is given by

$$\begin{aligned} \hat{\mathbf{x}}_{t|t} &= \mathbb{E}[\mathbf{x}_t|\mathbf{r}_{0:t}], \\ &= \int \mathbf{x}_t p(\mathbf{x}_t|\mathbf{r}_{0:t}) d\mathbf{x}_t. \end{aligned} \tag{5}$$

The conditional independence property of the system eqs. (2) – (4) enables for efficient *recursive* computation of this analysis pdf. Indeed, starting at time $t-1$ from $p(\mathbf{x}_{t-1}|\mathbf{r}_{0:t-1})$, one can compute $p(\mathbf{x}_t|\mathbf{r}_{0:t})$ following forecast and update steps as follows:

- *Forecast step.* The state transition pdf, $p(\mathbf{x}_t|\mathbf{x}_{t-1})$, is first used to compute the forecast pdf as (e.g., Ait-El-Fquih et al., 2016),

$$p(\mathbf{x}_t|\mathbf{r}_{0:t-1}) = \int p(\mathbf{x}_t|\mathbf{x}_{t-1}) p(\mathbf{x}_{t-1}|\mathbf{r}_{0:t-1}) d\mathbf{x}_{t-1}. \tag{6}$$

- *Update step with the GRACE TWS data.* Once available, the observation $\mathbf{y}_t$ is first used to update forecast pdf, $p(\mathbf{x}_t|\mathbf{r}_{0:t-1})$ as,

$$p(\mathbf{x}_t|\mathbf{r}_{0:t-1}, \mathbf{y}_t) \propto p(\mathbf{y}_t|\mathbf{x}_t) p(\mathbf{x}_t|\mathbf{r}_{0:t-1}), \tag{7}$$

and

$$p(\mathbf{x}_{t-1}|\mathbf{r}_{0:t-1}, \mathbf{y}_t) \propto p(\mathbf{y}_t|\mathbf{x}_{t-1})p(\mathbf{x}_{t-1}|\mathbf{r}_{0:t-1}). \tag{8}$$

While the likelihood $p(\mathbf{y}_t|\mathbf{x}_t)$ in the update (7) is given through the observation model, $p(\mathbf{y}_t|\mathbf{x}_{t-1})$ in (8) is not known and needs to be computed beforehand as,

$$p(\mathbf{y}_t|\mathbf{x}_{t-1}) = \int p(\mathbf{y}_t|\mathbf{x}_t)p(\mathbf{x}_t|\mathbf{x}_{t-1})d\mathbf{x}_t. \tag{9}$$

By ignoring the pseudo-observations, $\mathbf{z}_{0:t-1}$, in eqs. (7) – (8), these equations translate as a one-step-ahead (OSA) smoothing process, which computes the OSA smoothing pdf, $p(\mathbf{x}_{t-1}|\mathbf{y}_{0:t})$, from the previous analysis pdf $p(\mathbf{x}_{t-1}|\mathbf{y}_{0:t-1})$ (Ait-El-Fquih et al., 2016). For simplicity, we refer to pdf $p(\mathbf{x}_{t-1}|\mathbf{r}_{0:t-1}, \mathbf{y}_t)$ as the OSA smoothing pdf (note that the actual OSA smoothing pdfs are $p(\mathbf{x}_{t-1}|\mathbf{r}_{0:t})$, $p(\mathbf{x}_{t-1}|\mathbf{y}_{0:t})$ or $p(\mathbf{x}_{t-1}|\mathbf{z}_{0:t})$).

- *Update step with* $\mathbf{z}_t$. The pdf $p(\mathbf{x}_t|\mathbf{r}_{0:t-1}, \mathbf{y}_t)$ that stems from the update of the forecast pdf with $\mathbf{y}_t$ (eq. (7)) is in turn updated with $\mathbf{z}_t$ based on the Bayes' rule, leading to the analysis pdf of interest:

$$p(\mathbf{x}_t|\mathbf{r}_{0:t}) \propto p(\mathbf{z}_t|\mathbf{x}_t, \mathbf{y}_t, \mathbf{r}_{0:t-1})p(\mathbf{x}_t|\mathbf{r}_{0:t-1}, \mathbf{y}_t). \tag{10}$$

The unknown likelihood $p(\mathbf{z}_t|\mathbf{x}_t, \mathbf{y}_t, \mathbf{r}_{0:t-1})$ is computed beforehand as,

$$p(\mathbf{z}_t|\mathbf{x}_t, \mathbf{y}_t, \mathbf{r}_{0:t-1}) \approx \int p(\mathbf{z}_t|\mathbf{x}_t, \mathbf{x}_{t-1})p(\mathbf{x}_{t-1}|\mathbf{r}_{0:t-1}, \mathbf{y}_t)d\mathbf{x}_{t-1}. \tag{11}$$

3.2. The WCEnKF algorithm

In this section, the WCEnKF algorithm is described in three stages. The definition starts with the forecast step, in which the previous analysis ensemble state is integrated forward with the model to obtain the forecast ensemble. Two analysis (update) steps are then performed. The first updates, following a Kalman filter-like correction, the forecast ensemble based on the GRACE TWS data; the second update uses information of the water budget closure to perform a second Kalman filter-like correction, leading to the analysis ensemble of interest.

From previous section, it is not possible to analytically compute the integrals in eqs. (5) – (11) because of the nonlinearity of the model $\mathcal{M}(.)$. We therefore derive an EnKF solution (Evensen, 1994; Hoteit et al., 2015) by applying the standard random sampling properties 1 and 2 listed in

Appendix A. Starting at time $t-1$ from an analysis ensemble, $\{\mathbf{x}_{t-1}^{a,(i)}\}_{i=1}^{n}$, the analysis ensemble at next time (t), $\{\mathbf{x}_{t}^{a,(i)}\}_{i=1}^{n}$, can be computed by the following cycles of forecast and update steps.

- *Forecast step.* A forecast ensemble, $\{\mathbf{x}_{t}^{f,(i)}\}_{i=1}^{n}$, is first computed by integrating $\{\mathbf{x}_{t-1}^{a,(i)}\}_{i=1}^{n}$, forward in time with the model:

$$\mathbf{x}_t^{f,(i)} = \mathcal{M}_{t-1}(\mathbf{x}_{t-1}^{a,(i)}) + \nu^{(i)}, \tag{12}$$

where $\nu^{(i)}$ is a random sample from the Gaussian $\mathcal{N}(\mathbf{0}, \mathbf{Q}_t)$.

- *Update with GRACE TWS data (first update).* Once a new observation $\mathbf{y}_t$ is available, new ensemble $\{\tilde{\mathbf{x}}_{t}^{a,(i)}\}_{i=1}^{n}$ and $\{\tilde{\mathbf{x}}_{t-1}^{s,(i)}\}_{i=1}^{n}$ are then computed using an EnKF update of the forecast ensemble and the previous analysis ensemble:

$$\begin{aligned}
\mathbf{y}_t^{f,(i)} &= \mathbf{H}\mathbf{x}_t^{f,(i)} + \mathbf{w}^{(i)}; \quad \mathbf{w}^{(i)} \sim \mathcal{N}(\mathbf{0}, \mathbf{R}_t), && (13)\\
\tilde{\mathbf{x}}_t^{a,(i)} &= \mathbf{x}_t^{f,(i)} + \mathbf{P}_{\mathbf{x}_t^f}\mathbf{H}^T \underbrace{[\mathbf{H}\mathbf{P}_{\mathbf{x}_t^f}\mathbf{H}^T + \mathbf{R}_t]^{-1}[\mathbf{y}_t - \mathbf{y}_t^{f,(i)}]}_{\boldsymbol{\mu}_t^{(i)}}, && (14)\\
\tilde{\mathbf{x}}_{t-1}^{s,(i)} &= \mathbf{x}_{t-1}^{a,(i)} + \mathbf{P}_{\mathbf{x}_{t-1}^a, \mathbf{x}_t^f}\mathbf{H}^T\boldsymbol{\mu}_t^{(i)}. && (15)
\end{aligned}$$

The covariance matrices $\mathbf{P}_{\mathbf{x}_t^f}$ and $\mathbf{P}_{\mathbf{x}_{t-1}^a, \mathbf{x}_t^f}$, are evaluated beforehand from the previous analysis and forecast ensembles as,

$$\begin{aligned}
\mathbf{P}_{\mathbf{x}_t^f} &= (n-1)^{-1}\mathbf{S}_{\mathbf{x}_t^f}\mathbf{S}_{\mathbf{x}_t^f}^T, && (16)\\
\mathbf{P}_{\mathbf{x}_{t-1}^a, \mathbf{x}_t^f} &= (n-1)^{-1}\mathbf{S}_{\mathbf{x}_{t-1}^a}\mathbf{S}_{\mathbf{x}_t^f}^T, && (17)
\end{aligned}$$

where $\mathbf{S}_{\mathbf{x}_{t-1}^a}$ and $\mathbf{S}_{\mathbf{x}_t^f}$ are the perturbation matrices (i.e., matrices with n columns formed by the ensemble members minus the ensemble mean). Eqs. (14) and (15) are EnKF updates of $\mathbf{x}_t^{f,(i)}$ and $\mathbf{x}_{t-1}^{a,(i)}$, respectively. These updates are achieved based on $\mathbf{y}_t$, with Kalman gains $\mathbf{P}_{\mathbf{x}_t^f}\mathbf{H}^T[\mathbf{H}\mathbf{P}_{\mathbf{x}_t^f}\mathbf{H}^T + \mathbf{R}_t]^{-1}$ (eq. (14)) and $\mathbf{P}_{\mathbf{x}_{t-1}^a, \mathbf{x}_t^f}\mathbf{H}^T[\mathbf{H}\mathbf{P}_{\mathbf{x}_t^f}\mathbf{H}^T + \mathbf{R}_t]^{-1}$ (eq. (15)). The $\tilde{\mathbf{x}}_t^{a,(i)}$ is based on $\mathbf{y}_t$ only, and a second update with $\mathbf{z}_t$ is still required. The index '$\sim$' is used for the first update to distinguish it from the second one.

- *Adjustment with the water budget constraint (second update).* The pseudo-observation, $\mathbf{z}_t$, is then used to update $\{\tilde{\mathbf{x}}_{t}^{a,(i)}\}_{i=1}^{n}$, again using an EnKF update, leading to the actual state analysis ensemble of interest:

$$\mathbf{z}_t^{f,(i)} = \mathbf{G}\tilde{\mathbf{x}}_t^{a,(i)} + \mathbf{L}\tilde{\mathbf{x}}_{t-1}^{s,(i)} + \boldsymbol{\xi}_t^{(i)}; \quad \boldsymbol{\xi}_t^{(i)} \sim \mathcal{N}(\mathbf{0}, \boldsymbol{\Sigma}_t), \tag{18}$$

$$\mathbf{x}_t^{a,(i)} = \tilde{\mathbf{x}}_t^{a,(i)} + \mathbf{P}_{\tilde{\mathbf{x}}_t^a, \mathbf{z}_t^f}[\mathbf{N}\mathbf{P}_{\boldsymbol{\eta}_t}\mathbf{N}^T + \boldsymbol{\Sigma}_t]^{-1}[\mathbf{z}_t - \mathbf{z}_t^{f,(i)}], \tag{19}$$

with $\mathbf{N} = [\mathbf{G}, \mathbf{L}]$, the cross-covariance $\mathbf{P}_{\tilde{\mathbf{x}}_t^a, \mathbf{z}_t^f}$ is evaluated from the ensembles $\{\tilde{\mathbf{x}}_t^{a,(i)}\}_{i=1}^n$ and $\{\mathbf{z}_t^{f,(i)}\}_{i=1}^n$, as in eq. (17), and the covariance $\mathbf{P}_{\boldsymbol{\eta}_t}$ is computed from the augmented state ensemble $\{\boldsymbol{\eta}_t^{(i)}\}_{i=1}^n$, where $\boldsymbol{\eta}_t^{(i)} = [(\tilde{\mathbf{x}}_t^{a,(i)})^T, (\tilde{\mathbf{x}}_{t-1}^{s,(i)})^T]^T$, as in eq. (16). As one can see, eq. (19) translates an EnKF update of $\tilde{\mathbf{x}}_t^{a,(i)}$, based on the pseudo-observation $\mathbf{z}_t$, where gain is $\mathbf{P}_{\tilde{\mathbf{x}}_t^a, \mathbf{z}_t^f}[\mathbf{N}\mathbf{P}_{\boldsymbol{\eta}_t}\mathbf{N}^T + \boldsymbol{\Sigma}_t]^{-1}$, leading to $\mathbf{x}_t^{a,(i)}$, the state analysis ensemble of interest.

The PM eq. (5) estimate is then approximated by the sample mean of the resulting analysis ensemble. As discussed in the introduction, the pseudo-observations are only available at the discharge observations locations, but the Kalman update eq. (18) spreads the information to the whole state vectors. A schematic illustration of the filter algorithm is presented in Figure 3.

Similarly to the standard CEnKF of Pan et al. (2012), the proposed WCEnKF involves one forecast step and two successive update steps. The two filters have the same forecast and first update (with observation $\mathbf{y}_t$) steps, and only differ in their second update (adjustment with pseudo-observation $\mathbf{z}_t$)). The state update mechanism eqs. (18) – (19) is more general than the one in Pan et al. (2012), as the latter does not involve the OSA smoothing ensemble, $\{\tilde{\mathbf{x}}_{t-1}^{s,(i)}\}_i$ in eq. (18), eq. (19) and assume no noise ($\boldsymbol{\xi}_t^{(i)} = 0$) in eq. (18) and its covariance $\boldsymbol{\Sigma}_t = 0$ in eq. (19). As such, CEnKF can be considered as a direct particular case of WCEnKF. As stated above, accounting for uncertainties in the constraint allows avoiding a perfect pseudo-observation model scenario, which should help mitigating for over-fitting issues. The OSA smoothing terms (e.g., $\tilde{\mathbf{x}}_{t-1}^{s,(i)}$ in eq. (18)) come from the fact that the pseudo-observation, $\mathbf{z}_t$, in the constraint eq. (4) is not only function of $\mathbf{x}_t$ but also of $\mathbf{x}_{t-1}$.

FIGURE 3

3.3. Experimental Setup

All the water fluxes data (including **p**, **e**, and **q**) are accumulated to a monthly scale and used in the monthly assimilation processes. The monthly increment (i.e., the difference between the monthly averaged GRACE TWS and simulated TWS) can be added to each day of the current month, which guarantees that the update of the monthly mean is identical to the monthly mean of the daily updates. In practice, the differences between the predictions and the updated states are added as offsets to the state vectors at the last day of each month to generate the ensembles for the next month assimilation step. Given that not enough information are available to accurately estimate the pseudo-observation error covariance Σ, especially for **q**, to test the sensibility we consider the error values mentioned in Section 2.3 as *reference errors* and test with three different Σ: (1) the *reference errors* values minus 5% of observation values, (2) *reference errors*, and (3) the *reference errors* plus 5% of observation values. We further assume the observation errors to be spatially uncorrelated. This test allows us to analyze the influence of the pseudo-observations on the final results.

To generate an initial ensemble to start the filtering process, we follow Renzullo et al. (2014) and perturb the meteorological forcing fields. To this end, we assume a Gaussian multiplicative error of 30% for precipitation, an additive Gaussian error of $50Wm^{-2}$ for the shortwave radiation, and a Gaussian additive error of $2°C$ for temperature (Jones et al., 2007; Renzullo et al., 2014). The initial ensemble is then computed by sampling the above Gaussian distributions (see details in Renzullo et al., 2014). We, then, integrate the resulting ensemble (with 30 members) forward with the model from January 2000 to April 2002 to generate the initial ensembles at the beginning of the study period. An ensemble of 30 members is selected as it was found large enough to obtain sufficient ensemble spread at reasonable computational cost.

We further apply ensemble inflation and localization to enhance the filters performances (e.g., Anderson et al., 2007). These techniques were proven to be useful in dealing with neglected uncertainties in the system and small ensembles (e.g., Hamill and Snyder, 2002; Bergemann and Reich, 2010). Ensemble inflation with a best case coefficient factor of 1.12 (after testing different values) is applied here to increase the ensemble deviation from the ensemble-mean (Anderson et al., 2007). Local Analysis (LA) (Evensen, 2003) is used to restrict the impact of the measurements in the update step to variables located within a certain distance only (5° as suggested by Khaki et al., 2017b). By spatially limiting the influences of observations over large distances in the sample covariance, LA can help mitigating spatial correlation errors and rank deficiency problem during the assimilation (see Khaki et al., 2017b, for more details). This is particularly useful to account for the spatial correlation errors in satellite products, particularly GRACE (Khaki et al., 2017b; Tangdamrongsub et al., 2017).

4. Results

We first investigate the effects of different scenarios applied for errors associated with the fluxes in Section 4.1. In Section 4.2, we evaluate the performance of WCEnKF against in-situ groundwater measurements over the Mississippi River Basin in the US and the Murray-Darling Basin in Australia. To further assess the behavior of the proposed WCEnKF, we compare its results with the standard EnKF for predicting water storages. Then, in Section 4.3, we analyze the assimilation results and the performance of the proposed filter in enforcing the balance between water fluxes, e.g., we assess the behaviour of the filters in dealing with water balance problem.

4.1. Error Sensitivity Analysis

We first analyze the effects of the different datasets, i.e., both the GRACE TWS and pseudo-observations on the filter estimates. The incorporation of the pseudo-observations in the second update step of the filter modifies the contribution of GRACE TWS data on the state estimations. As such, the three different covariance error matrices (cf. Section 3.3) of $\mathbf{p}$, $\mathbf{e}$, and $\mathbf{q}$ would cause that both the GRACE TWS and pseudo-observations contribute differently. For each grid point, we calculate the correlations between the filter estimations of TWS and the water fluxes $\mathbf{p}$, $\mathbf{e}$, and $\mathbf{q}$ as well as the assimilated GRACE TWS data. The results along with the average imbalance errors (from the water balance equation) are presented in Table 2. It can be seen that applying the first case with minimum error values, as it is expected, leads to a higher correlation between the filter estimates and other water fluxes. The least imbalance error is also achieved in this case. However, in general, increasing the impact of water fluxes in the second step of the filter decreases the correlation between the estimates and GRACE TWS data. This suggests, as we expected, a trade-off between the effects of observations in the first and second step of the filter according to the values of Σ. In the third scenario, for example, applying pseudo-observations with larger errors leads to smaller correlations with the water flux observations and larger correlation to the GRACE TWS data. Note that we also applied a similar test for $\mathbf{p}$, $\mathbf{e}$, and $\mathbf{q}$ with zero error (such that CEnKF), which resulted in the least imbalance error. Nevertheless, this case leads to larger errors compared to groundwater measurements compared with the three scenarios above. Therefore, hereafter, we only present the results associated with the second scenario (with no additional errors on those that are initially assumed). This case is found to lead to better results when groundwater estimates from each scenario are compared to independent groundwater in-situ measurements (details in Section 4.2).

TABLE 2

4.2. Assessment against In-situ Data

The estimated groundwater storage obtained from each filter is compared to the post-processed in-situ measurements of groundwater changes (cf. Section 2.4) over the Mississippi Basin and Murray-Darling Basin. To this end, the estimated groundwater storages, as well as model-free run (without data assimilation) are spatially interpolated to the location of the in-situ measurements using the nearest neighbour (the closest four grid values). The groundwater misfits (errors) between the in-situ measurements and those of the EnKF and WCEnKF are then computed. Figures 4 and 5 plot the resulting bias, namely, differences between groundwater estimated by the filters and in-situ measurements, and STD (of the calculated differences) for the Mississippi Basin and Murray-Darling Basin, respectively.

FIGURE 4

FIGURE 5

For both basins, the estimated biases are significantly decreased when the proposed WCEnKF filter is applied. The average estimated bias using WCEnKF is 23.14 mm for the Mississippi Basin and 26.89 mm for the Murray-Darling Basin, indicating an average of 22.10% and 26.38% bias improvements compared to the EnKF. Despite this, we found that the correlation between the filters' estimated groundwater and in-situ groundwater time series are large for both basins. An average of 0.76 (at 95% confidence interval) for both basins is achieved, which means that assimilating only GRACE data (as in the EnKF) is good for estimating annual and inter-annual variations, but not enough to accurately recover their amplitudes. The error reduction using WCEnKF is also noticeable in the STD. WCEnKF decreases the uncertainties in the Mississippi Basin and Murray-Darling Basin by 48.87% and 35.19%, respectively.

For every grid point within each basin, we calculate the Root-Mean-Squared Error (RMSE) and also the correlation between in-situ measurements and filters results. Note that cross-correlation is applied to account for lag differences between the time series. We further undertake a significance test for the correlation coefficients using t-distribution. The estimated t-value and the distribution at 0.05 significant level are then used to calculate a p-value. The calculated p-values for the correlations in Table 3 lie under 5% indicating coefficients are significant. Table 3 summarizes these results. The Assimilation of the GRACE data using WCEnKF increases the correlation from 0.72 (EnKF) to 0.84 over the Mississippi Basin and from 0.68 to 0.79 for the Murray-Darling Basin. While both filters significantly improve groundwater estimates with respect to model-free run (48.13 on average), the larger RMSE improvements of 15.02% and 16.71% for the Mississippi Basin and the Murray-Darling Basin, respectively, suggest the enhancement gained from the proposed two-updates filter against the one-update filter.

TABLE 3

Furthermore, two analyses are undertaken on the forecast steps to investigate which filter is more efficient in keeping observations effects within the system states. Generally, a filter with better forecasts can perform better during an experiment. We calculate average RMSE of groundwater estimates at forecast steps for the Mississippi and Murray-Darling Basins and compare them with those of model-free run (Table 4). It can be seen that both filters reduced RMSE values, while WCEnKF outperforms the EnKF scheme (approximately 12%). We also compute correlations between TWS forecast estimates, both by filters and model-free, and water fluxes (i.e., **p**, **e**, and **q**). A similar analysis as Table 3 is done to control the significance of correlation coefficients. Average correlations over the basins of Amazon, Indus, Mississippi, Orange, Danube, St. Lawrence, Murray-Darling, and the Yangtze (cf. Figure 1) are listed in Table 4. Based on the correlation values, it is evident that WCEnKF achieves larger correlations with respect to the EnKF. The proposed filter obtains improved agreement between the assimilation results and the fluxes.

Furthermore, to statistically investigate the difference between average correlation values, ANOVA (analysis of variance; Nelson, 1983; Ullman, 1989) method is applied. The method shows how mean values are different. For every flux correlation, the null hypothesis is that the average correlation for the model-free, EnKF, and WCEnKF are equal. ANOVA tests the above hypothesis at 0.05 significance level. Our experiment indicates that the means are not equal, thus, ANOVA in the second step determines which correlations are different (to the level of significance). After implementing the later step, the EnKF result demonstrates a significantly larger difference from the model-free and WCEnKF. In sum, Table 4 shows that WCEnKF successfully assimilates data sets into the system, which also leads to a better forecast.

TABLE 4

4.3. Water Balance Enforcement

In the following, we analyze the results of the filter estimates using the second scenario from Section 4.1 in terms of their relationship to the observations and more importantly water budget closure. Figure 6 shows the results for the comparison between the assimilation results and GRACE TWS data. For each grid point, we calculate the average discrepancy and correlation between the two TWS time series. Results indicate that the error between the model and GRACE data is about 26 mm, which is 69% less than those resulting from the free-run (model runs without assimilation) and 13% higher than data assimilation results using the (one-update) EnKF scheme. This means that the application of the second update step, in some cases, decreases the effects of GRACE data by enforcing the balance between water fluxes. Figure 6b, in general, suggests a high correlation between the filter estimates and observations. Nevertheless, again, smaller correlations are found in places with a denser discharge stations corresponding to better imbalance control (e.g., central to northern of Asia). Much smaller correlations are observed between GRACE TWS and the model-only results (0.47 on average). Nevertheless, the EnKF provides 11% higher correlation to observations. This is due to the effects of the second update step of the proposed filter.

FIGURE 6

The above results could be explained by the correlations between the filter estimates and two water fluxes data, i.e., precipitation and evaporation. Indeed, as one can see in Figure 7, the locations where a high correlation is achieved, are places where the second step of the filter affects more due to the availability of discharge data (cf. Figure 1). Approximately 33% and 44% larger correlation coefficients for **p** and **e**, respectively, are achieved in the areas where water balance adjustment is used compared with other areas. This illustrates that forcing water balance condition into the assimilation process increases the agreement between model outputs and other water fluxes on the one hand, and may change the effects of the GRACE data on the model on the other hand.

FIGURE 7

The average imbalance at each grid point is plotted in Figure 8. The figure clearly demonstrates how the water budget enforcement spatially influences the imbalance between Δs and fluxes. It can be seen that wherever a dense network of water discharge stations exists (cf. Figure 1), e.g., North America, Southeast Asia, and West Australia, a smaller imbalance between all compartments occurs. For other areas, the imbalance is much larger because the second analysis step of WCEnKF cannot be applied due to the lack of discharge data and the method simply performs as the EnKF. Therefore, this highlights the effect of the second step of WCEnKF in dealing with imbalances. This confirms the previous results that the second update step in WCEnKF increases the agreement between the assimilation outputs and the water fluxes, which results in water imbalance decreases.

FIGURE 8

TABLE 5

Table 5 summarizes the average correlations between the estimated TWS data and water fluxes, **p**, **e** and **q**, and the average estimated imbalance errors as suggested by the EnKF and WCEnKF. Note that we only compare the filters' performances over the points in which discharge data is available. WCEnKF successfully increases the correlation between the results and water variables of **p**, **e** and **q** with average improvements of 33%, 44%, and 45%, respectively. This leads to a significant imbalance reduction of approximately 82% (suggesting an error of 18.31 mm compared to 62.17 mm for the EnKF).

Next, in order to further investigate the data assimilation results, we focus on the major basins of Amazon, Indus, Mississippi, Orange, Danube, St. Lawrence, Murray-Darling, and the Yangtze (cf. Figure 1). Due to variability of various water fluxes over different areas, these have different characteristics and behaviors with various contributions through the second update of the filter (Figure 9). Figure 9 illustrates the contribution of each water flux in the water budget closure of the basins. This shows how each variable incorporates in the water balance equation differently over each basin. Generally the larger contributions are found for $\mathbf{p}$ and $\mathbf{e}$ for all basins. $\mathbf{q}$ has a larger contribution over the Amazon Basin and relatively small impacts on the Orange Basin and St. Lawrence Basin. The estimated water storage change ($\Delta\mathbf{s}$) effects, however, vary significantly between the basins. It is shown in Figure 9 that $\Delta\mathbf{s}$ has larger influences over Mississippi, Danube, and Murray-Darling Basins. The share of $\Delta\mathbf{s}$ in each basin is affected by incorporating $\mathbf{p}$, $\mathbf{e}$ and $\mathbf{q}$ into the second step of WCEnKF, which is significantly different from the one estimated by the EnKF.

FIGURE 9

Figure 10 presents the average $\Delta\mathbf{s}$ as they result from the EnKF and WCEnKF over each basin. It can be seen that the application of water balance adjustment in the filtering process results in a considerable difference between the estimated TWSs. The larger correlations between the two solutions in the Mississippi Basin (0.50) and St. Lawrence Basin (0.47) indicate less influence of the water budget constraint in these basins. However, the weak agreements between the EnKF and WCEnKF results, with about 0.34 correlation on average, suggest a large impact of water balance enforcement on the process. This remarkable difference is expected to have a large effect on imbalance issue for each basin (Figure 11).

FIGURE 10

The spatial average time series of imbalance between Δs and fluxes for each basin are shown in Figure 11 for the EnKF and WCEnKF. In all the cases, the new filter successfully decreases the imbalance in comparison to the EnKF. The EnKF results in larger water balance problem in the Mississippi and Danube basins, while the proposed WCEnKF suggests the best performances over these two basins with average imbalance reductions of 87% and 84%, respectively. We also compute the standard deviation (STD) of each time series (cf. Figure 11). The large range of calculated STD in the EnKF (10.9 mm) is reduced to 5.64 mm by applying WCEnKF. Furthermore, the proposed filter appropriately improves disagreement between all compartments, both in terms of magnitudes and STDs. Figure 11 further suggests the importance of implementing the water balance adjustment. The absolute (average) imbalance without using this approach is 67.08 mm, and a large part of it is directly connected to the estimated TWS. The WCEnKF data assimilation decreases this value to approximately 14.45 mm, which leads to both better estimation of TWS and higher agreement with the other water fluxes.

FIGURE 11

5. Summary and Conclusions

GRACE TWS data are assimilated into W3RA covering 2002 – 2012 to improve model outputs and satisfy the terrestrial water budget balance. For that purpose, we propose a two-update weak constrained EnKF (WCEnKF) scheme that enforces water budget closure using the water fluxes. WCEnKF shows a good performance in integrating GRACE TWS data into the system (first update) and constraining the water balance equation (second update). Larger correlations in terms of groundwater estimates are found between assimilation results using the two-update filter (14.10% average) and ground-based observations, compared with those of the model-free. We also achieve 21.12% (on average) groundwater RMSE reductions using WCEnKF compared with EnKF. The application of the proposed filter shows an ability in imposing the water budget closure constraint as demonstrated by higher correlation of the estimated TWS changes to the $\mathbf{p}$, $\mathbf{e}$, and $\mathbf{q}$ (0.33, 0.44, and 0.45, respectively), as well as an imbalance reduction, i.e., from 62.17 mm using the traditional EnKF, to 18.31 mm (82.53% improvement).

There are some key factors that affect the performance of WCEnKF. Most importantly errors associated with pseudo-observations can largely alter the results. It is very difficult to achieve spatio-temporal variations of error characteristics of each water budget component. This study assesses three different error scenarios and investigates their impact on the results. However, the assumptions that are made, especially using a fixed uncertainty, might be inappropriate or sometimes strong since various data sets have performed differently within different areas. Therefore, more investigations are still needed to fully assess the filter's capability in terms of data uncertainties, applying multiple data sets for each variable (e.g., $\mathbf{p}$, $\mathbf{e}$), and using other types of observations such as soil moisture for data assimilation.

Acknowledgement

We would like to thank Dr. Natthachet Tangdamrongsub for his useful comments, which contributed to the improvement of this study. M. Khaki is grateful for the research grant of Curtin International Postgraduate Research Scholarships (CIPRS)/ORD Scholarship provided by Curtin University (Australia). This work is a TIGeR publication.

Appendix A. Some useful properties of random sampling

Property 1 (Hierarchical sampling; Robert, 2006). Assuming that one can sample from $p(\mathbf{x}_1)$ and $p(\mathbf{x}_2|\mathbf{x}_1)$, then a sample, $\mathbf{x}_2^*$, from $p(\mathbf{x}_2)$ can be generated by drawing $\mathbf{x}_1^*$ from $p(\mathbf{x}_1)$ and then $\mathbf{x}_2^*$ from $p(\mathbf{x}_2|\mathbf{x}_1^*)$.

Property 2 (Conditional sampling; Hoffman et al., 1991). Consider a Gaussian pdf, $p(\mathbf{x}, \mathbf{y})$, with $\mathbf{P}_{xy}$ and $\mathbf{P}_y$ denoting the cross-covariance of $\mathbf{x}$ and $\mathbf{y}$ and the covariance of $\mathbf{y}$, respectively. Then a sample, $\mathbf{x}^*$, from $p(\mathbf{x}|\mathbf{y})$, can be generated as, $\mathbf{x}^* = \widetilde{\mathbf{x}} + \mathbf{P}_{xy}\mathbf{P}_y^{-1}[\mathbf{y} - \widetilde{\mathbf{y}}]$, where $(\widetilde{\mathbf{x}}, \widetilde{\mathbf{y}}) \sim p(\mathbf{x}, \mathbf{y})$.

Appendix B. Derivation of the WCEnKF algorithm

The equation (12), which computes the forecast ensemble $\{\mathbf{x}_t^{f,(i)}\}_{i=1}^n$ from the previous analysis one, is obtained by applying Prop. 1 above to the forecast step (6). Regarding the first update step (with $\mathbf{y}_t$), one first applies Prop. 1 on the following formula,

$$p(\mathbf{y}_t|\mathbf{r}_{0:t-1}) = \int \underbrace{p(\mathbf{y}_t|\mathbf{x}_t)}_{\mathcal{N}(\mathbf{H}_t\mathbf{x}_t, \mathbf{R}_t)} p(\mathbf{x}_t|\mathbf{r}_{0:t-1})d\mathbf{x}_t,$$

to sample the observation forecast ensemble, $\{\mathbf{y}_t^{f,(i)}\}_{i=1}^n$, as in eq. (13). Prop. 2 is then used in eqs. (7) to obtain the ensembles $\{\tilde{\mathbf{x}}_t^{a,(i)}\}_{i=1}^n$ (eq. (14)) and $\{\mathbf{x}_{t-1}^{s,(i)}\}_{i=1}^n$, respectively. For the second update step (with $\mathbf{z}_t$), one first uses Prop. 1 in eq. (11), with $p(\mathbf{z}_t|\mathbf{x}_t, \mathbf{x}_{t-1}) \overset{(4)}{=} \mathcal{N}(\mathbf{G}\mathbf{x}_t + \mathbf{L}\mathbf{x}_{t-1}, \mathbf{\Sigma}_t)$, to obtain the pseudo-observation forecast ensemble $\{\mathbf{z}_t^{f,(i)}\}_{i=1}^n$ (eq. (18)), then Prop. 2 in eq. (10) to compute the state analysis ensemble $\{\mathbf{x}_t^{a,(i)}\}_{i=1}^n$ (eq. (19)).

References

Aires, F. (2014). Combining datasets of satellite retrieved products. Part I: Methodology and water budget closure. Journal of Hydrometeorology, 15 (4), 16771691.

Ait-El-Fquih, B., El Gharamti, M., Hoteit, I., (2016)a. A Bayesian consistent dual ensemble Kalman filter for state-parameter estimation in subsurface hydrology, Hydrol. Earth Syst. Sci., 20, 3289-3307, http://dx.doi.org/10.5194/hess-20-3289-2016.

Ait-El-Fquih, B., Hoteit, I., (2016)b. A Variational Bayesian Multiple Particle Filtering Scheme for Large-Dimensional Systems, in IEEE Transactions on Signal Processing, vol. 64, no. 20, pp. 5409-5422, Oct.15, 15 2016. http://dx.doi.org/10.1109/TSP.2016.2580524.

Alsdorf, D.E., Rodriguez, E., Lettenmaier, D.P., (2007). Measuring surface water from space, Rev. Geophys., 45, RG2002, http://dx.doi.org/10.1029/2006RG000197.

Anderson, J., Anderson, S., (1999). A Monte Carlo implementation of the nonlinear filtering problem to produce ensemble assimilations and forecasts. Mon. Weather Rev. 127, 27412758.

Anderson, M.C., Norman, J.M., Mecikalski, J.R., Otkin, J.A., Kustas, W.P., (2007). A climatological study of evapotranspiration and moisture stress across the continental United States based on thermal remote sensing: 1. Model formulation. J. Geophys. Res. 112 (D10117). http://dx.doi.org/10.1029/2006JD007506.

Bergemann, K., Reich, S., (2010). A mollified ensemble Kalman filter. Q.J.R. Meteorol. Soc., 136: 16361643. http://dx.doi.org/10.1002/qj.672.

Bertino, L., Evensen G., Wackernagel, H., (2003). Sequential Data Assimilation Techniques in Oceanography, International Statistical Review, Vol. 71, No. 2 (Aug., 2003), pp. 223-241.

Boyer, J.F., Dieulin, C., Rouchie, N., Cres, A., Servat, E., Paturel, J.E.,Mahe, G., (2006). SIEREM an environmental information system for water resources. 5th World FRIEND Conference, La Havana - Cuba, November 2006 in Climate Variability and Change Hydrological Impacts IAHS Publ. 308, p19-25.

Brocca, L., Melone, F., Moramarco, T., Wagner, W., Naeimi, V., Bartalis, Z., Hasenauer, S., (2010). Improving runoff prediction through the assimilation of the ASCAT soil moisture product, Hydrol. Earth Syst. Sci., 14, 18811893, http://dx.doi.org/10.5194/hess-14-1881-2010.

Chen, M., Shi, W., Xie, P., Silva, V.B.S., Kousky, V.E., Wayne Higgins, R., Janowiak, J.E., (2008). Assessing objective techniques for gauge-based analyses of global daily precipitation, J. Geophys. Res., 113, D04110, http://dx.doi.org/10.1029/2007JD009132.

Cheng, M.K., Tapley, B.D., (2004). Variations in the Earth's oblateness during the past 28 years. Journal of Geophysical Research, Solid Earth, 109, B09402. http://dx.doi.org/10.1029/2004JB003028.

Chiew, F.H.S., Stewardson, M.J., McMahon, T.A., (1993). Comparison of six rainfall-runoff modelling approaches, J. Hydrol., 147, 136.

Döll, P., Kaspar, F., Lehner, B., (2003). A global hydrological model for deriving water availability indicators: model tuning and validation, J. Hydrol., 270, 105134.

Eicker, A., Schumacher, M., Kusche, J., Dll, P., Mller-Schmied, H., (2014). Calibration/data assimilation approach for integrating GRACE data into the WaterGAP global hydrology model (WGHM) using an ensemble Kalman filter: first results, SurvGeophys, 35(6):12851309. http://dx.doi.org/10.1007/s10712-014-9309-8.

Eicker, A., Forootan, E., Springer, A., Longuevergne, L., Kusche J., (2016). Does GRACE see the terrestrial water cycle intensifying?, J. Geophys. Res. Atmos., 121, 733745, http://dx.doi.org/10.1002/2015JD023808.

Evensen, G., (1994). Sequential data assimilation with a nonlinear quasi-geostrophic model using Monte Carlo methods to forecast error statistics, J. Geophys. Res., 99, 10, 14310, 162.

Evensen, G., (2003). The ensemble Kalman filter: Theoretical formulation and practical inplementation, Ocean Dynamics, 53, 343367, http://dx.doi.org/10.1007/s10236-003-0036-9.

Ferguson, C.R., Sheffield, J., Wood, E.F., Gao, H., (2010). Quantifying uncertainty in a remote sensing-based estimate of evapotranspiration over the continental United States, Int. J. Rem. Sens., 31, pp. 3821-3865, http://dx.doi.org/10.1080/01431161.2010.483490.

Forootan, E., Didova, O., Schumacher, M, Kusche, J., Elsaka, B., (2014). Comparisons of atmospheric mass variations derived from ECMWF reanalysis and operational fields, over 2003 to 2011. Journal of Geodesy, 88, Pages 503-514, http://dx.doi.org/10.1007/s00190-014-0696-x.

Garcia, M., Hoar, T., Thomas, M., Bailey, B., Castillo, J., (2016). Interfacing an ensemble Data Assimilation system with a 3D nonhydrostatic Coastal Ocean Model, an OSSE experiment, OCEANS 2016 MTS/IEEE Monterey, Monterey, CA, 2016, pp. 1-11, http://dx.doi.org/10.1109/OCEANS.2016.7760992.

Gharamti, M.E., Ait-El-Fquih, B., Hoteit, I., (2015). An iterative ensemble Kalman filter with one-step-ahead smoothing for state-parameters estimation of contaminant transport models, Journal of Hydrology, Volume 527, August 2015, Pages 442-457, ISSN 0022-1694, https://doi.org/10.1016/j.jhydrol.2015.05.004.

Gharamti, M.E., Valstar, J., Janssen, G., Marsman, A., Hoteit, I., (2016). On the efficiency of the hybrid and the exact second-order sampling formulations of the EnKF: a reality-inspired 3-D test case for estimating biodegradation rates of chlorinated hydrocarbons at the port of Rotterdam, Hydrol. Earth Syst. Sci., 20, 4561-4583, http://dx.doi.org/10.5194/hess-20-4561-2016, 2016.

Giustarini, L., Matgen, P., Hostache, R., Montanari, M., Plaza, D., Pauwels, V.R.N., De Lannoy, G.J.M., De Keyser, R., Pfister, L., Hoffmann, L., Savenije, H.H.G., (2011). Assimilating SAR-derived water level data into a hydraulic model: a case study, Hydrol. Earth Syst. Sci., 15, 23492365, http://dx.doi.org/10.5194/hess-15-2349-2011.

Gutentag, E.D., Heimes, F.J., Krothe, N.C., Luckey, R.R., Weeks, J.B., (1984). Geohydrology of the High Plains aquifer in parts of Colorado, Kansas, Nebraska, New Mexico, Oklahoma, South Dakota, Texas, and Wyoming, U.S. Geol. Surv. Prof. Pap., 1400-B, 66 pp.

Hamill, T.M., Snyder, C., (2002). Using improved background-error covariances from an ensemble Kalman filter for adaptive observations. Mon Wea Rev 130:15521572. http://dx.doi.org/10.1175/1520-0493(2002)130¡1552:UIBECF¿2.0.CO;2.

Henck, A.H., Montgomery, D.R., Huntington, K.W., Liang, C., (2010). Monsoon control of effective discharge, Yunnan and Tibet, Geology, v. 38, p. 975-978.

Hoffman, Y., Ribak, E., (1991). Constrained realizations of Gaussian fields - A simple algorithm, Astrophysical Journal, Part 2 - Letters (ISSN 0004-637X), vol. 380, Oct. 10, 1991, p. L5-L8.

Hoteit, I., Luo, X., Pham, D.T., (2012). Particle Kalman Filtering: A Nonlinear Bayesian Framework for Ensemble Kalman Filters, Monthly Weather Review, 140:2, 528-542.

Hoteit, I., Pham, D.T., Gharamti, M. E., Luo, X., (2015). Mitigating Observation Perturbation Sampling Errors in the Stochastic EnKF, Monthly Weather Review, 143:7, 2918-2936.

Huffman, G., Adler, R., Arkin, P., Chang, A., Ferraro, R., Gruber, A., Janowiak, J., McNab, A., Rudolf, B., Schneider, U., (1997). The Global Precipitation Climatology Project (GPCP) Combined Precipitation Dataset. Bull. Amer. Meteor. Soc., 78, 520, http://dx.doi.org/10.1175/1520-0477(1997)078¡0005:TGPCPG¿2.0.CO;2.

Huffman, G.J., Adler, R.F., Bolvin, D.T., Gu, G., Nelkin, E.J., Bowman, K.P., Hong, Y., Stocker, E.F., Wolff, D.B., (2007). The TRMM Multi-satellite Precipitation Analysis: Quasi- Global, Multi-Year, Combined-Sensor Precipitation Estimates at Fine Scale. J. Hydrometeor., 8(1), 38-55.

Huntington, T.G., (2006). Evidence for intensification of the global water cycle: Review and synthesis, J. Hydrol.,319(14), 8395, http://dx.doi.org/10.1016/j.jhydrol.2005.07.003.

Jones, D.A., Wang, W., Fawcett, R., Grant, I., (2007). Climate data for the Australian water availability project. In: Australian Water Availability Project Milestone Report. Bur. Met., Australia, 37pp.

Khaki, M., Hoteit, I., Kuhn, M., Awange, J., Forootan, E., van Dijk, A.I.J.M., Schumacher, M., Pattiaratchi, C., (2017a). Assessing sequential data assimilation techniques for integrating GRACE data into a hydrological model, Advances in Water Resources, Volume 107, Pages 301-316, ISSN 0309-1708, http://dx.doi.org/10.1016/j.advwatres.2017.07.001.

Khaki, M., Schumacher, M., J., Forootan, Kuhn, M., Awange, E., van Dijk, A.I.J.M., (2017b). Accounting for Spatial Correlation Errors in the Assimilation of GRACE into Hydrological Models through localization, Advances in Water Resources, Available online 1 August 2017, ISSN 0309-1708, https://doi.org/10.1016/j.advwatres.2017.07.024.

Kumar, S.V., Peters-Lidard, C.D., Santanello, J.A., Reichle, R.H., Draper, C.S., Koster, R.D., Nearing, G., Jasinski, M.F., (2015). Evaluating the utility of satellite soil moisture retrievals over irrigated areas and the ability of land data assimilation methods to correct for unmodeled processes, Hydrology and Earth System Sciences, 19, 4463-4478, http://dx.doi.org/10.5194/hess-19-4463-2015.

Kusche, J., Schmidt R., Petrovic, S., Rietbroek, R., (2009). Decorrelated GRACE time-variable gravity solutions by GFZ and their validation using a hydrological model, Journal of Geodesy, http://dx.doi.org/10.1007/s00190-009-0308-3.

Liu, C., Xue, M., (2016). Relationships among Four-Dimensional Hybrid EnsembleVariational Data Assimilation Algorithms with Full and Approximate Ensemble Covariance Localization. Mon. Wea. Rev., 144, 591606, http://dx.doi.org/10.1175/MWR-D-15-0203.1.

Liu, Y., Peters-Lidard, C.D., Kumar, S., Foster, J.L., Shaw, M., Tian, Y., Fall, G.M., (2013). Assimilating satellitebased snow depth and snow cover products for improving snow predictions in Alaska, Adv. Water Res., 54, 208227, http://dx.doi.org/10.1016/j.advwatres.2013.02.005.

Mayer-Gürr, T., Zehentner, N., Klinger, B., Kvas, A., (2014). ITSG-Grace2014: a new GRACE gravity field release computed in Graz. - in: GRACE Science Team Meeting (GSTM), Potsdam am: 29.09.2014.

McLaughlin, D., (2002). An integrate approach to hydrologic data assimilation: Interpolation, smoothing, and filtering, Adv. Water Resour., 25, 12751286.

Mu, Q., Heinsch, F.A., Zhao, M., Running, S.W., (2007). Development of a global evapotranspiration algorithm based on MODIS and global meteorology data. Remote Sensing of Environment 111, 519-536, http://dx.doi.org/10.1016/j.rse.2007.04.015.

Mu, Q., Zhao, M., Running, S.W., (2011). Improvements to a MODIS Global Terrestrial Evapotranspiration Algorithm. Remote Sensing of Environment 115: 1781-1800.

Munier, S., Aires, F., Schlaffer, S., Prigent, C., Papa, F., et al., (2014). Combining datasets of satellite retrieved products for basin-scale water balance study. Part II: Evaluation on the Mississippi Basin and closure correction model. Journal of Geophysical Research: Atmospheres, American Geophysical Union, 2014, 119, pp.100-116.

Neal, J., Schumann, G., Bates, P., Buytaert, W., Matgen, P., Pappenberger, F., (2009). A data assimilation approach to discharge esti- mation from space, Hydrol. Process., 23, 36413649.

Nelson, P.R., (1983). A Comparison of Sample Sizes for the Analysis of Means and the Analysis of Variance, Journal of Quality Technology, 15, pp.3339.

Ott, E., Hunt, B.R., Szunyogh, I., Zimin, A.V., Kostelich, E.J., Corazza, M., Kalnay, E., Patil, D.J., Yorke, J.A., (2004). A local ensemble Kalman Filter for atmospheric data assimilation. Tellus, 56A: 415-428.

Pan, M., Wood, E.F., (2006). Data assimilation for estimating the terrestrial water budget using a constrained ensemble Kalman filter. Journal of Hydrometeorology, 7 (3), 534547.

Pan, M., Sahoo, A.K., Troy, T.J., Vinukollu, R.K., Sheffield, J., Wood, E.F., (2012). Multisource Estimation of Long-Term Terrestrial Water Budget for Major Global River Basins. Journal of Climate, 25 (9), 31913206.

Ramoelo, A., Majozi, N., Mathieu, R., et al., (2014). Validation of global evapotranspiration product (MOD16) using flux tower data in the African savanna, South Africa. Remote Sensing, 6 (8), 7406-7423.

Reichle, R.H., McLaughlin, D.B., Entekhabi, D., (2002). Hydrologic Data Assimilation with the Ensemble Kalman Filter. Mon. Wea. Rev. 130, 103114, http://dx.doi.org/10.1175/1520-0493(2002)130¡0103:HDAWTE¿2.0.CO;2.

Renzullo, L.J., Van Dijk, A.I.J.M., Perraud, J.M., Collins, D., Henderson, B., Jin, H., Smith, A.B., McJannet, D.L., (2014). Continental satellite soil moisture data assimilation improves root-zone moisture analysis for water resources assessment. J. Hydrol., 519, 27472762. http://dx.doi.org/10.1016/j.jhydrol.2014.08.008.

Roads, J., , et al., (2003). GCIP water and energy budget synthesis (WEBS). J. Geophys. Res., 108, 8609, http://dx.doi.org/10.1029/2002JD002583.

Robert, C., (2006). Le choix baysien, Springer-Verlag Paris, ISSN 978-2-287-25173-3.

Rodell, M., Houser, P., Jambor, U., Gottschalck, J., Mitchell, K., Meng, C., Arsenault, K., Cosgrove, B., Radakovich, J., Bosilovich, M., Entin, J., Walker, J., Lohmann, D., Toll, D., (2004). The Global Land Data Assimilation System. Bull. Amer. Meteor. Soc., 85, 381394, http://dx.doi.org/10.1175/BAMS-85-3-381.

Rodell, M., Chen, J., Kato, H., Famiglietti, J.S., Nigro, J., Wilson, C.R., (2007). Estimating groundwater storage changes in the Mississippi River basin (USA) using GRACE, Hydrogeol. J., 15, 159166.

Sahoo, A.K., Pan, M., Troy, T.J., Vinukollu, R.K., Sheffield, J., Wood, E.F., (2011). Reconciling the global terrestrial water budget using satellite remote sensing. Remote Sensing of Environment, 115 (8), 1850-1865.

Schmidt, A.H., Montgomery, D.R., Huntington, K.W., Liang, C., (2011). The Question of Communist Land Degradation: New Evidence from Local Erosion and Basin-Wide Sediment Yield in Southwest China and Southeast Tibet, Annals of the Association of American Geographers,, First published on: 28 March 2011 (iFirst)

Schumacher M., Eicker, A., Kusche, J., Schmied, H.M., Dll, P., (2015). Covariance Analysis and Sensitivity Studies for GRACE Assimilation into WGHM. In: Rizos C., Willis P. (eds) IAG 150 Years, International Association of Geodesy Symposia, vol 143. Springer, Cham.

Schumacher, M., Kusche, J., Dll, P., (2016). A systematic impact assessment of GRACE error correlation on data assimilation in hydrological models, Journal of Geodesy, http://dx.doi.org/10.1007/s00190-016-0892-y.

Seo, D.J., Koren, V., Cajina, N., (2003). Real-time variational assimilation of hydrologic and hydrometeorological data into operational hydrologic forecasting. J. Hydrometeorol., 4, 627641.

Seoane, L., Ramillien, G., Frappart, F., Leblanc, M., (2013). Regional GRACE-based estimates of water mass variations over Australia: validation and interpretation, Hydrol. Earth Syst. Sci., 17, 4925-4939, http://dx.doi.org/10.5194/hess-17-4925-2013.

Sheffield, J., Goteti, G., Wood, E.F., (2006). Development of a 50-yearhigh-resolution global dataset of meteorological forcings for land surfacemodeling, J. Clim., 19(13), 30883111.

Sheffield, J., Ferguson, C.R., Troy, T.J., Wood, E.F., McCabe, M.F., (2009). Closing the terrestrial water budget from satellite remote sensing. Geophysical Research Letter, 26, L07403, http://dx.doi.org/10.1029/2009GL037338.

Sokolov, A.A., Chapman, T.G., (1974). Methods for Water Balance Computation An International Guide for Research and Practice, The Unesco Press, Paris.

Stewart, L.M., Dance, S.L., Nichols, N.K., (2008). Correlated observation errors in data assimilation. Int. J. Numer. Meth. Fluids, 56: 15211527. http://dx.doi.org/10.1002/fld.1636.

Smith, P.J., Dance, S.L., Nichols, N.K., (2011). A hybrid data assimilation scheme for model parameter estimation: Application to morphodynamic modelling, Computers and Fluids, Volume 46, Issue 1, July 2011, Pages 436-441, ISSN 0045-7930, http://dx.doi.org/10.1016/j.compfluid.2011.01.010.

Swenson, S., Chambers, D., Wahr, J., (2008). Estimating geocentervariations from a combination of GRACE and ocean model output. Journal of Geophysical research, 113, B08410, http://dx.doi.org/10.1029/2007JB005338.

Tangdamrongsub, N., Steele-Dunne, S.C., Gunter, B.C., Ditmar, P.G., and Weerts, A.H., (2015). Data assimilation of GRACE terrestrial water storage estimates into a regional hydrological model of the Rhine River basin, Hydrol. Earth Syst. Sci., 19, 2079-2100, http://dx.doi.org/10.5194/hess-19-2079-2015.

Tangdamrongsub, N., Steele-Dunne, S.C., Gunter, B.C., Ditmar, P.G., Sutanudjaja, E.H., Xie, T, Wang, Z., (2017). Improving estimates of water resources in a semi-arid region by assimilating GRACE data into the PCR-GLOBWB hydrological model, Hydrology and Earth System Sciences, 21, 2053-2074.

Tian, S., Tregoning, P., Renzullo, L.J., van Dijk, A.I.J.M., Walker, J.P., Pauwels, V.R.N., Allgeyer, S., (2017). Improved water balance component estimates through joint assimilation of GRACE water storage and SMOS soil moisture retrievals, Water Resour. Res., 53, http://dx.doi.org/10.1002/2016WR019641.

Tregoning, P., McClusky, S., van Dijk, A.I.J.M., Crosbie, R.S., Pea-Arancibia, J.L., (2012). Assessment of GRACE Satellites for Groundwater Estimation in Australia, National Water Commission, Canberra, 82 pp.

Tropical Rainfall Measuring Mission (TRMM), (2011). TRMM (TMPA/3B43) Rainfall Estimate L3 1 month 0.25 degree x 0.25 degree V7, Greenbelt, MD, Goddard Earth Sciences Data and Information Services Center (GES DISC), Accessed [Data Access Date] https://disc.gsfc.nasa.gov/datacollection/TRMM_3B43_7.html.

Ullman, N.R., (1989). The Analysis of Means (ANOM) for Signal and Noise, Journal of Quality Technology, 21, pp.111127.

van Dijk, A.I.J.M., (2010). The Australian Water Resources Assessment System: Technical Report 3, Landscape model (version 0.5) Technical Description, CSIRO: Water for a Healthy Country National Research Flagship.

van Dijk, A.I.J.M., Renzullo, L.J., and Rodell, M., (2011). Use of Gravity Recovery and Climate Experiment terrestrial water storage retrievals to evaluate model estimates by the Australian water resources assessment system, Water Resour. Res., 47, W11524, http://dx.doi.org/10.1029/2011WR010714.

van Dijk, A.I.J.M., Pea-Arancibia, J.L., Wood, E.F., Sheffield, J., Beck, H.E., (2013). Global analysis of seasonal streamflow predictability using an ensemble prediction system and observations from 6192 small catchments worldwide, Water Resour. Res., 49, 27292746, http://dx.doi.org/10.1002/wrcr.20251.

van Dijk, A.I.J.M., Renzullo, L.J., Wada, Y., Tregoning, P., (2014). A global water cycle reanalysis (20032012) merging satellite gravimetry and altimetry observations with a hydrological multi-model ensemble. Hydrol Earth Syst Sci 18:29552973. http://dx.doi.org/10.5194/hess-18-2955-2014.

Vrugt, J.A., Diks, C.G., Gupta, H.V., Bouten, W., Verstraten, J.M., 2005. Improved treatment of uncertainty in hydrologic modeling: Combining the strengths of global optimization and data assimilation. Water Resour. Res, 41, W01017, http://dx.doi.org/10.1029/2004WR003059.

Vrugt, J.A., ter Braak, C.J.F., Diks, C.G.H., Schoups, G., (2013). Advancing hydrologic data assimilation using particle Markov chain Monte Carlo simulation: theory, concepts and applications, Advances in Water Resources, Anniversary Issue - 35 Years, 51, 457-478, http://dx.doi.org/10.1016/j.advwatres.2012.04.002.

Wahr, J.M., Molenaar, M., Bryan, F., (1998). Time variability of the Earth's gravity field: hydrological and oceanic effects and their possible detection using GRACE. J Geophys Res 108(B12):3020530229, http://dx.doi.org/10.1029/98JB02844.

Wooldridge, S.A., Kalma, J.D., (2001). Regional-scale hydrological modelling using multiple-parameter landscape zones and a quasi-distributed water balance model. Hydrological Earth System Sciences. 5: 59-74.

Zaitchik, B.F., Rodell, M., Reichle, R.H., (2008). Assimilation of GRACE terrestrial water storage data into a land surface model: results for the Mississippi River Basin. J Hydrometeorol 9(3):535548, http://dx.doi.org/10.1175/2007JHM951.1.

Zhang, Y., Pan, M., Wood, E.F., (2016). On Creating Global Gridded Terrestrial Water Budget Estimates from Satellite Remote Sensing. Surveys in Geophysics, 37 (2), 249268.

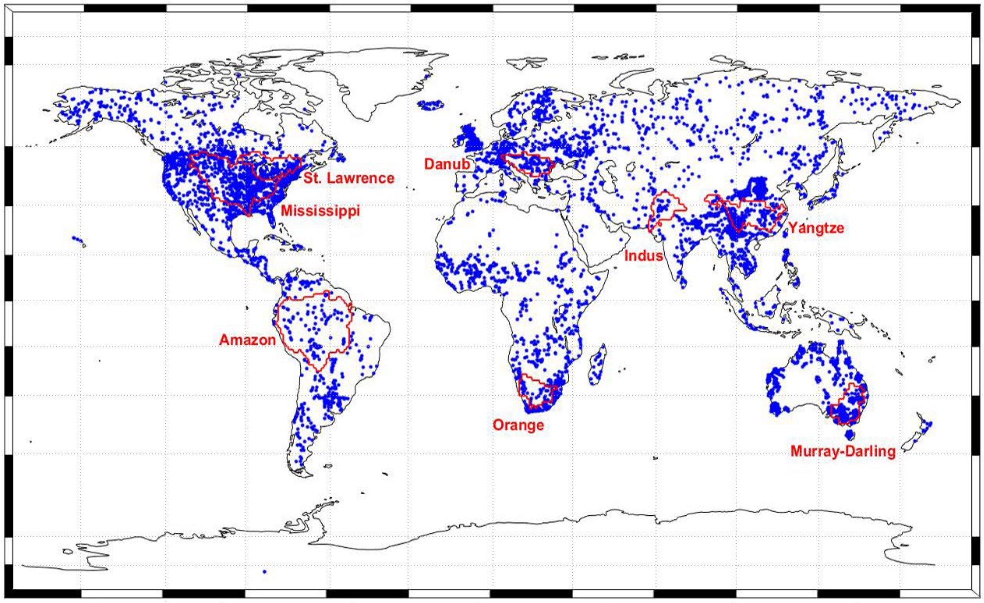

Figure 1: Distribution of water discharge stations used in this study.

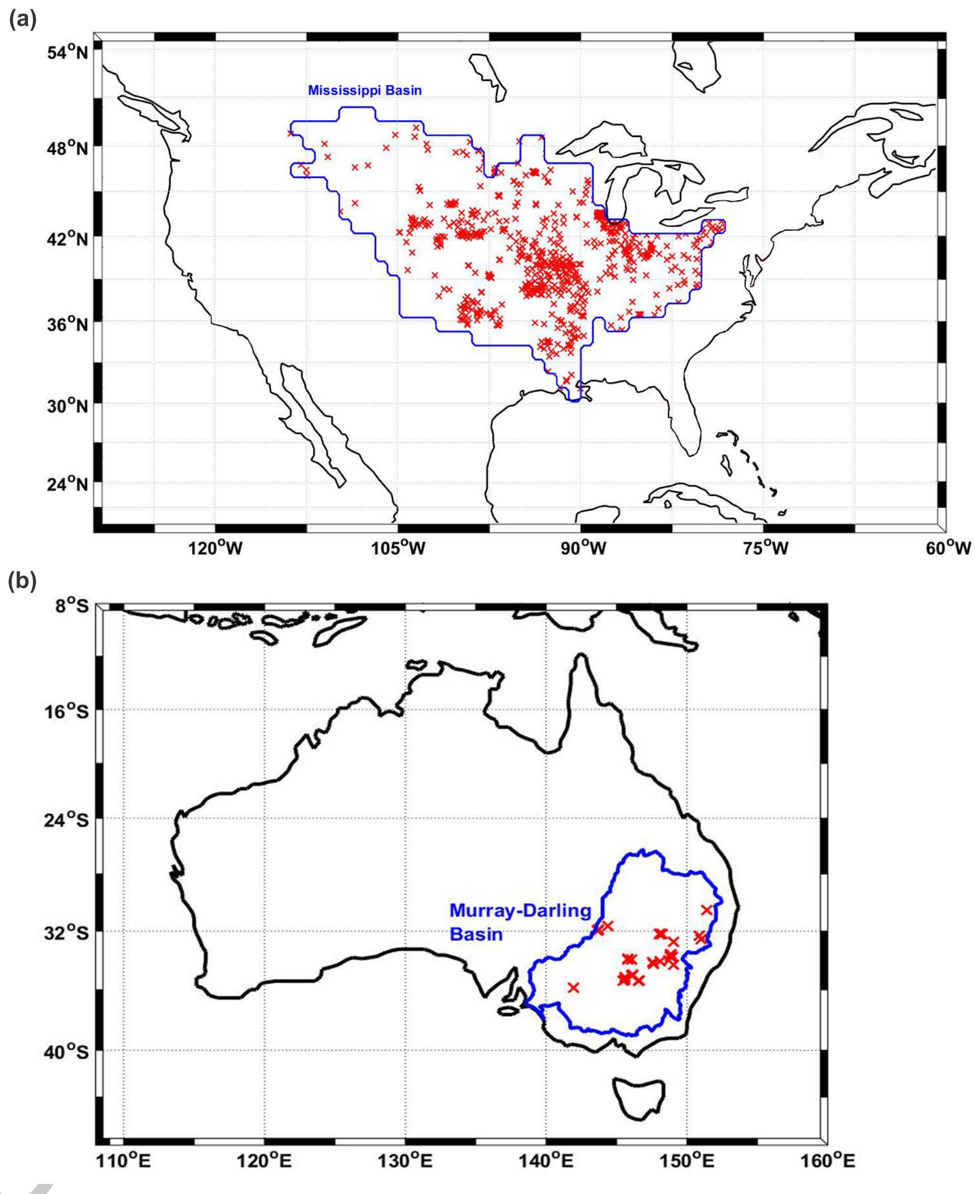

Figure 2: Locations of groundwater stations within (a) the Mississippi Basin in the US (a) and (b) the Murray-Darling Basin in Australia.

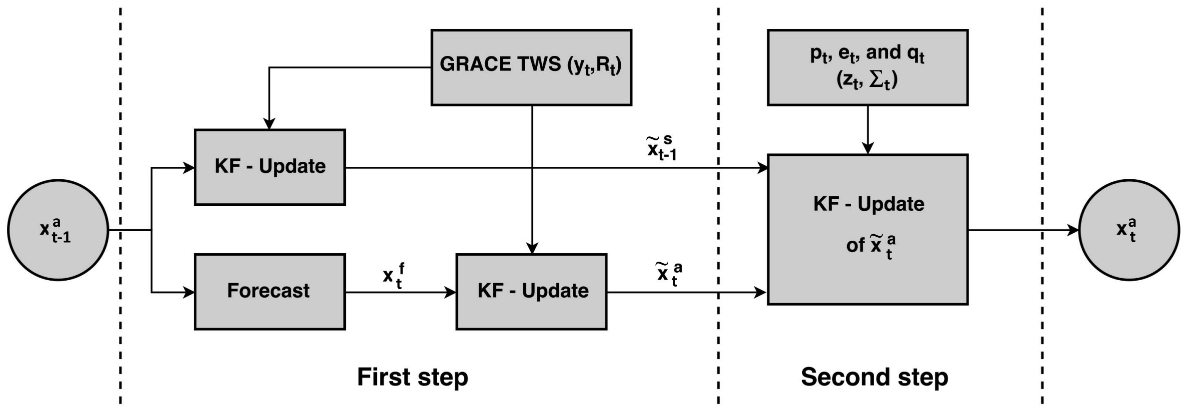

Figure 3: A schematic illustration of the WCEnKF filter's steps applied for data assimilation in this study.

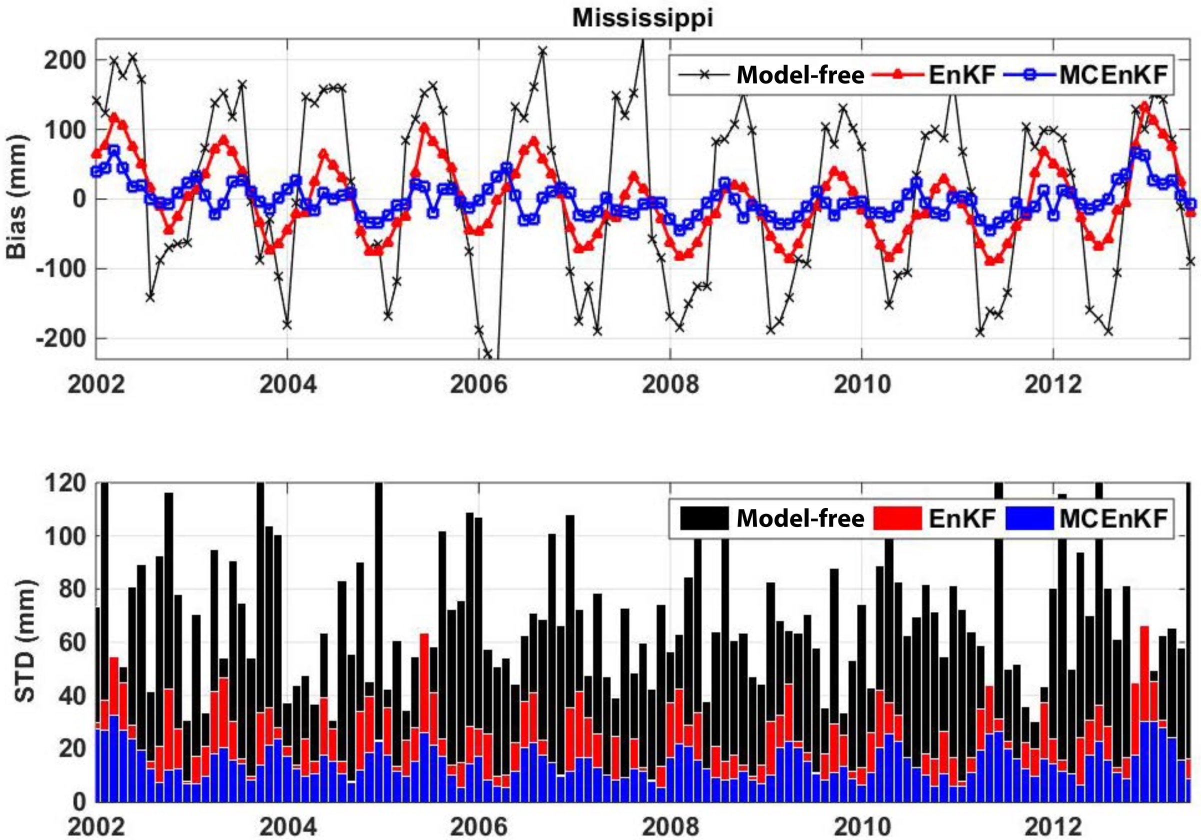

Figure 4: Average bias and STD of the groundwater results from the EnKF and WCEnKF data assimilation filters over the Mississippi Basin with respect to the in-situ groundwater measurements.

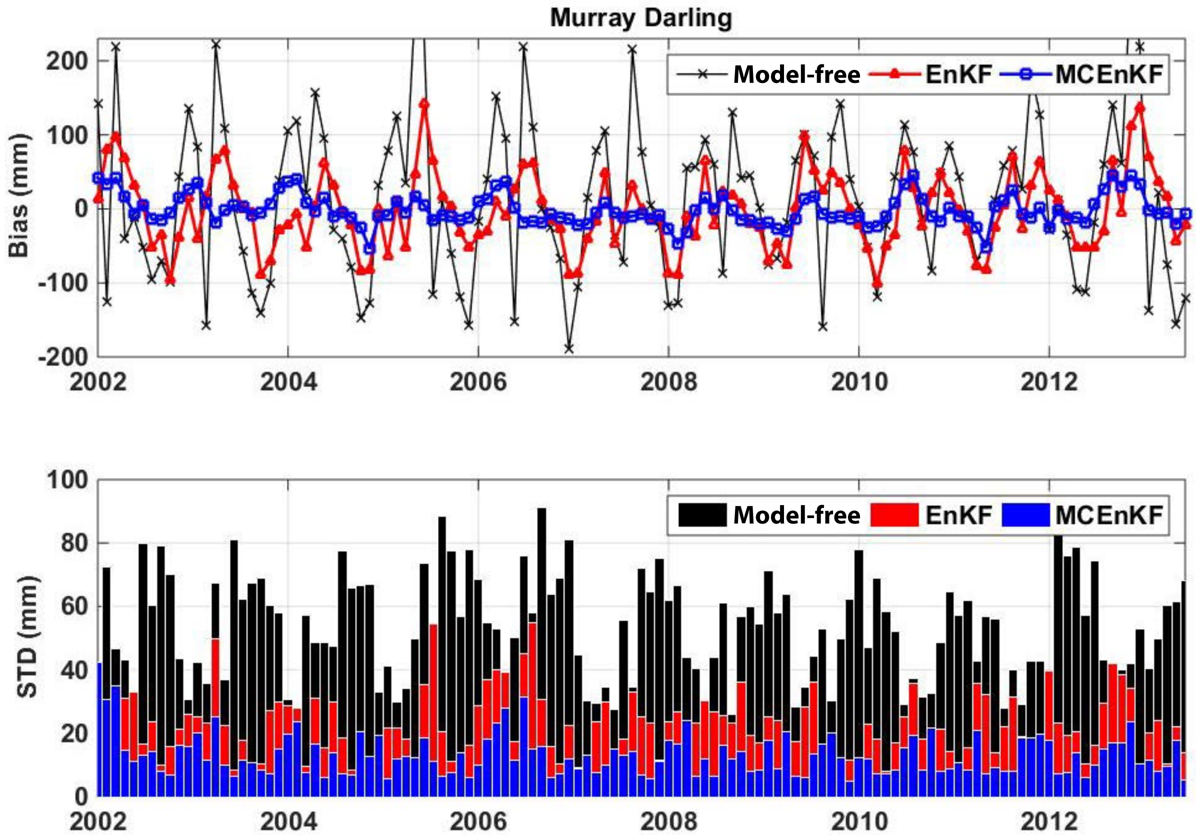

Figure 5: Average bias and STD of the groundwater results from the EnKF and WCEnKF data assimilation filter over the Murray-Darling Basin with respect to the in-situ groundwater measurements.

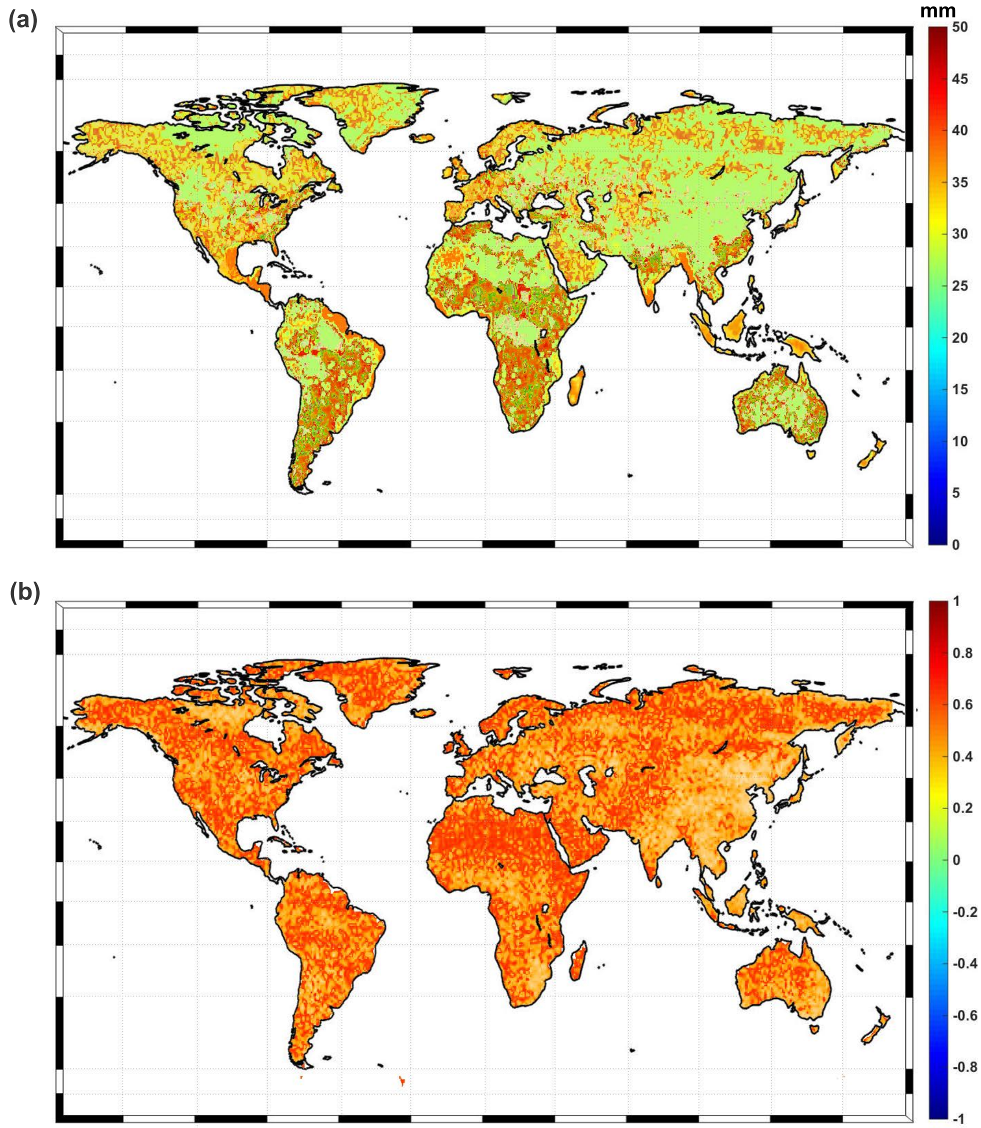

Figure 6: (a), Temporal average of misfits between the summation of TWS from WCEnKF and the GRACE TWS time series at each grid point, and (b), The correlation between the two TWS time series.

(a)

(b)

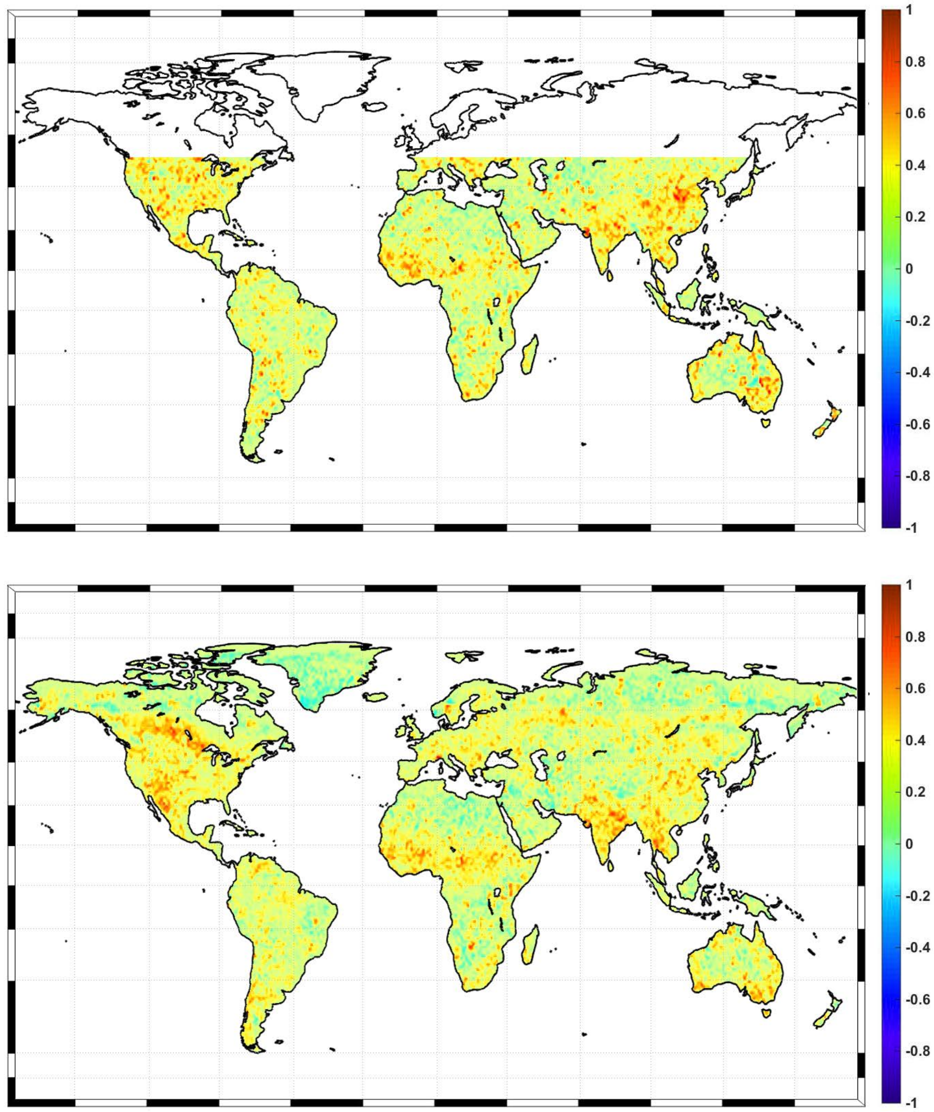

Figure 7: Correlation between the data assimilation results and **p** (a) and **e** (b) time series at each grid point.

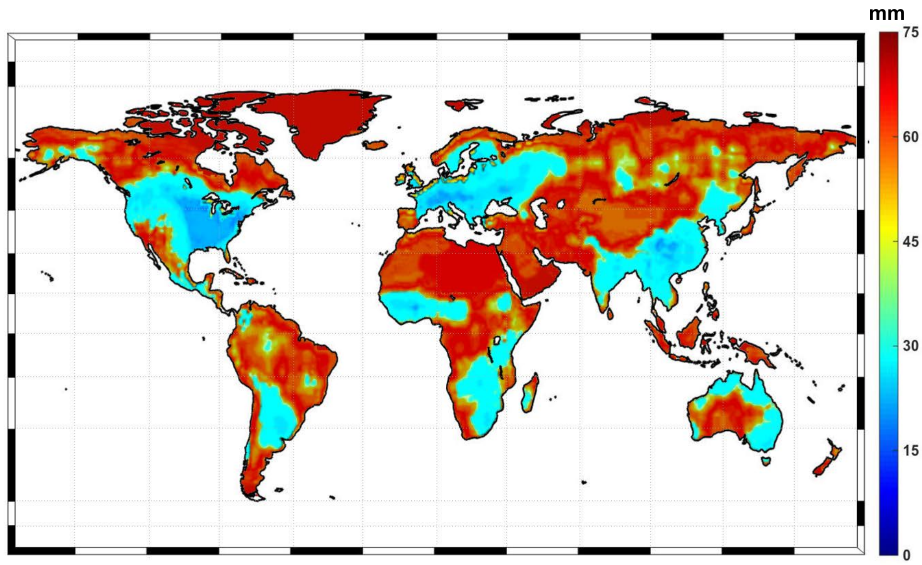

Figure 8: Temporal average of imbalance errors.

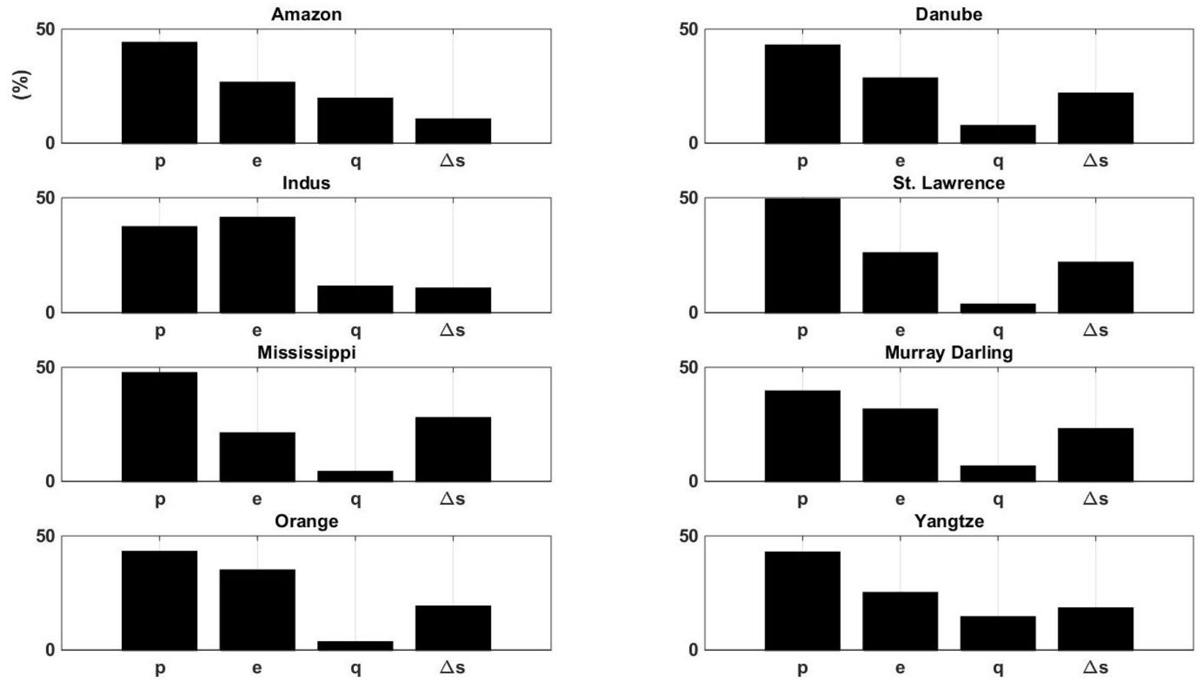

Figure 9: Contributions of each water flux in water budget closure over different basins.

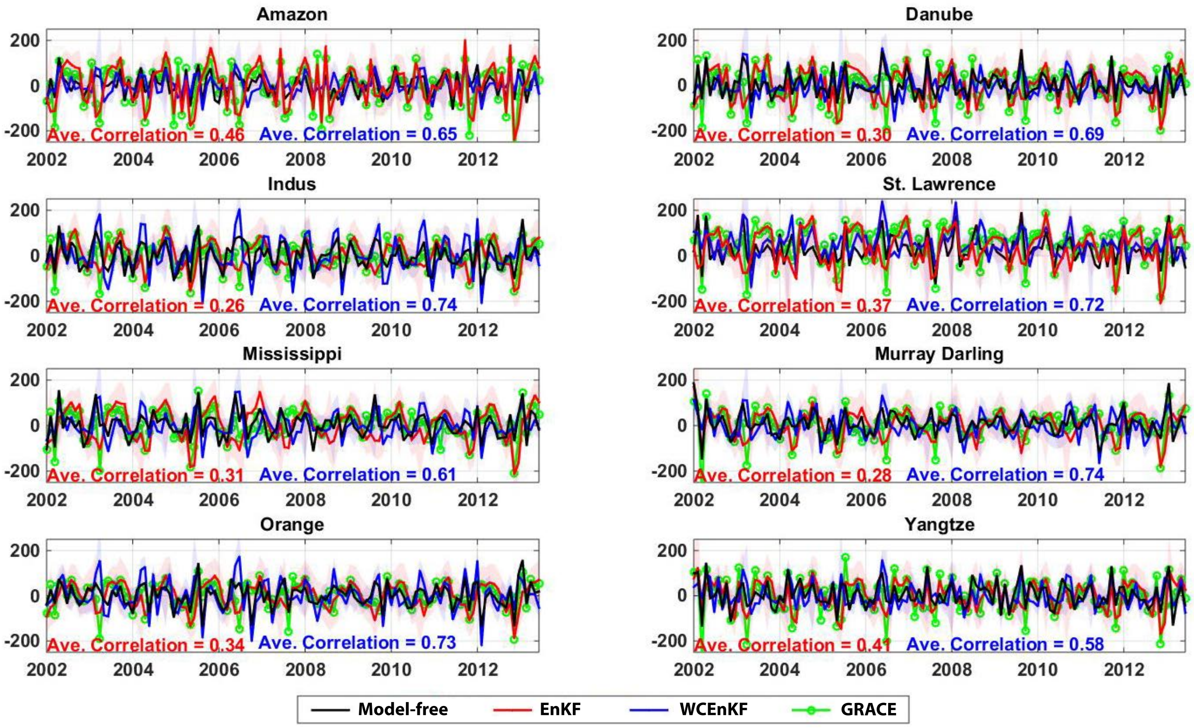

Figure 10: Spatial average time series of $\Delta \mathbf{s}$ from each filter over different basins (units are mm). Shaded areas represent ensemble spreads of water storage change time series. Correlation values of WCEnKF and EnKF are depicted on the figure.

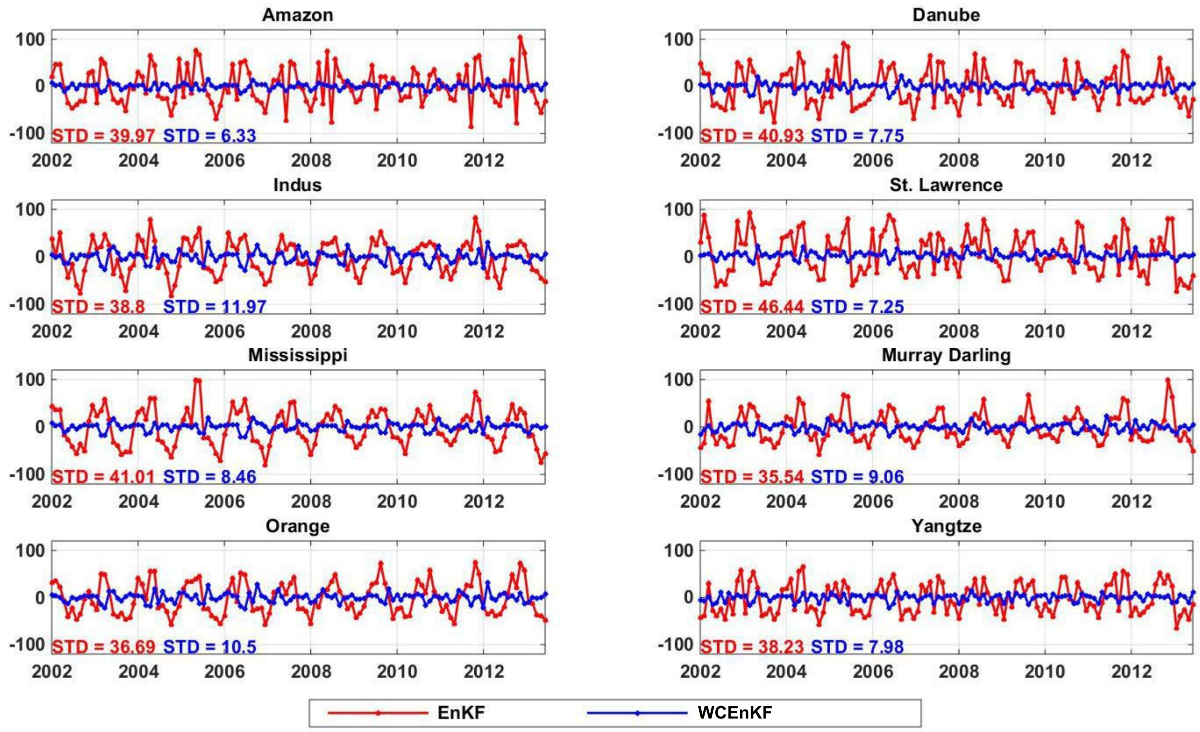

Figure 11: Average imbalance error time series calculated using the EnKF and WCEnKF filters for each basin (units are mm).

Table 1: A summary of the datasets used in this study.

Description	Platform	Data access
Terrestrial water storage (TWS)	GRACE	https://www.tugraz.at/institute/ifg/downloads/gravity-field-models/itsg-grace2014/
Daily accumulated precipitation (**p**)	TRMM-3B42	http://disc2.gesdisc.eosdis.nasa.gov/data/TRMM_L3/TRMM_3B42_Daily.7
MODIS Global Evapotranspiration (**e**)	MOD16	http://www.ntsg.umt.edu/project/mod16
Water discharge (**q**)	GRDC	http://www.bafg.de/GRDC/EN/Home/homepage_node.html
q		http://www.hydrosciences.fr/sierem/consultation/choixaccess.asp?lang=en
q	USGS	https://waterdata.usgs.gov/nwis/sw
q		http://www.bom.gov.au/waterdata/
q	NRFA	http://nrfa.ceh.ac.uk/data/
q		http://www.ore-hybam.org/
q		http://www.hydrology.gov.np/new/bull3/index.php/hydrology/home/main
Hydrological model	W3RA	http://www.wenfo.org/wald/data-software/
Groundwater in-situ measurements	USGS	https://water.usgs.gov/ogw/data.html
	NSW	http://waterinfo.nsw.gov.au/pinneena/gw.shtml

Table 2: Average correlations and errors between the water storages estimated by WCEnKF and water fluxes observations of **p**, **e** and **q** as well as GRACE TWS data considering three different error values used in the data assimilation process. "Ref" in table refers to the *reference errors* (described in Section 3.3)

Error level	Correlation				Imbalance error (mm)
	p	**e**	**q**	**GRACE TWS**	
(1) Ref-5%(observation)	0.78	0.83	0.76	0.77	12.05
(2) Ref+0%(observation)	0.65	0.72	0.69	0.84	18.31
(3) Ref+5%(observation)	0.61	0.63	0.58	0.89	37.24

Table 3: Summary of the evaluation results from each filter and model-free run against the groundwater in-situ measurements over the Mississippi Basin and Murray-Darling Basin. For each case the RMSE average and its range (±XX) at the 95% confidence interval is presented.

	Mississippi Basin		Murray-Darling Basin	
Method	**RMSE (mm)**	**Correlation**	**RMSE (mm)**	**Correlation**
EnKF	56.74±6.12	0.72	41.58±6.48	0.68
Improvement (%) regarding model-free	38.41	36.11	48.96	47.06
WCEnKF	48.22±5.63	0.84	34.63±5.27	0.79
Improvement (%) regarding model-free	47.66	45.23	57.49	54.43
Improvement (%) regarding EnKF	15.02	14.28	16.71	13.92

Table 4: Average RMSE results (with their ranges ±XX at the 95% confidence) by each filter at forecast steps and model-free run compared to the groundwater in-situ measurements over the Mississippi Basin and Murray-Darling Basin. Table also contains correlations between TWS estimated by the methods at forecast steps and water fluxes.

	RMSE (mm)		Correlation		
Method	**Mississippi Basin**	**Murray-Darling Basin**	**p**	**e**	**q**
Model-free	92.13±12.39	81.46±10.67	0.95	0.86	0.83
EnKF	74.53±8.82	62.71±9.25	0.56	0.53	0.49
WCEnKF	65.48±7.18	47.91±7.95	0.94	0.82	0.85

Table 5: Average correlation between the assimilation results (summation of water storages) and the data of **p**, **e** and **q**. The average imbalance errors provided by each filtering method are also indicated.

Method	Correlation			Imbalance error (mm)
	p	**e**	**q**	
EnKF	0.32	0.28	0.24	62.17
WCEnKF	0.65	0.72	0.69	18.31
Improvement (%)	50.76	61.11	65.21	70.55

A Two-update Ensemble Kalman Filter for Land Hydrological Data Assimilation with an Uncertain Constraint

M. Khaki[a,1], B. Ait-El-Fquih[b], I. Hoteit[b], E. Forootan[c], J. Awange[a], M. Kuhn[a]

[a]Department of Spatial Sciences, Curtin University, Perth, Australia.

[b]King Abdullah University of Science and Technology (KAUST), Thuwal, Saudi Arabia.

[c]School of Earth and Ocean Sciences, Cardiff University, Cardiff, UK.

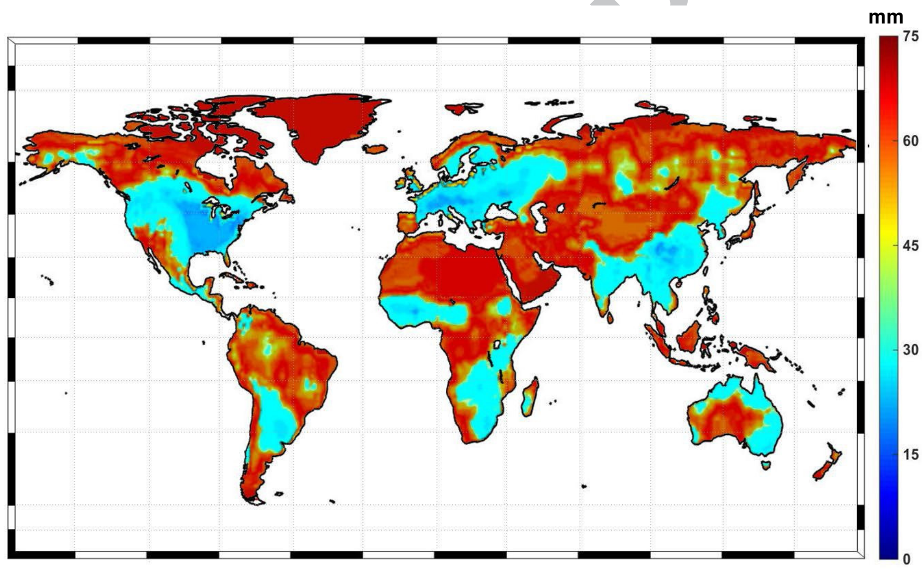

Temporal average of imbalance errors.

In the present study, a new constrained ensemble Kalman filter, which we refer to as weak constrained ensemble Kalman filter (WCEnKF), is introduced that satisfies the closure of the water balance equation. The proposed WCEnKF contains two update steps; it first incorporates observations from Gravity Recovery And Climate Experiment (GRACE) to improve model simulations of water storages, and second, it uses the additional climatic observations of precipitation, evaporation, and also ground-based water discharge to establish the water budget closure.

Highlights:

- We propose a new data assimilation filtering technique called a weak constrained ensemble Kalman filter (WCEnKF)
- We assimilate GRACE data to improve a hydrological model estimations
- The water budget closure is impose in the filtering process
- Independent in-situ measurements are used to evaluate the results
- WCEnKF significantly decreased the water budget imbalance error